Mitochondrial alterations triggered by repeated exposure to fine (PM2.5-0.18) and quasi-ultrafine (PM0.18) fractions of ambient particulate matter

J. Sotty, J. Kluza, C. de Sousa, M. Tardivel, S. Anthérieu, L.-Y. Alleman, L. Canivet, E. Perdrix, A. Loyens, P. Marchetti, et al.

MITOCHONDRIAL ALTERATIONS TRIGGERED BY REPEATED EXPOSURE TO FINE ($PM_{2.5-0.18}$) AND QUASI-ULTRAFINE ($PM_{0.18}$) FRACTIONS OF AMBIENT PARTICULATE MATTER

Sotty J.[1], Kluza J.[2], De Sousa C.[1], Tardivel M.[3], Antherieu S. [1], Alleman L-Y[4], Canivet L.[1], Perdrix E.[4], Loyens, A.[5], Marchetti P.[2], Lo Guidice J-M.[1], Garçon G.[1]

[1] Univ. Lille, CHU Lille, Institut Pasteur de Lille, ULR 4483-IMPECS, 59000 Lille, France

[2] Univ. Lille, CNRS, Inserm, CHU Lille, Institut de Recherche contre le Cancer de Lille, UMR 9020-UMR-S 1277 - Canther - Cancer Heterogeneity, Plasticity and Resistance to Therapies, 59000 Lille, France

[3] Univ. Lille, BioImaging Centre Lille-Nord de France (BICeL), 59000, Lille, France

[4] IMT Lille Douai, Univ. Lille, SAGE - Département Sciences de l'Atmosphère et Génie de l'Environnement, 59000 Lille, France

[5] University of Lille, Inserm, CHU Lille, UMR-S 1172 - Lille Neuroscience & Cognition, 59000 Lille, France.

Corresponding Author: Guillaume GARÇON, Univ. Lille, CHU Lille, Institut Pasteur de Lille, ULR 4483-IMPECS, 59000 Lille, France; E-mail: guillaume.garcon@univ-lille.fr

ABSTRACT

Nowadays ambient particulate matter (PM) levels still regularly exceed the guideline values established by World Health Organization in most urban areas. Numerous experimental studies have already demonstrated the airway toxicity of the fine fraction of PM (FP), mainly triggered by oxidative stress-induced airway inflammation. However, only few studies have actually paid close attention to the ultrafine fraction of PM (UFP), which is likely to be more easily internalized in cells and more biologically reactive. Mitochondria are major endogenous sources of reactive oxygen species (ROS) through oxidative metabolism, and coordinate many critical cellular signaling processes. Mitochondria have been often studied in the context of PM toxicity and generally associated with apoptosis activation. However, little is known about the underlying adaptation mechanisms that could occur following exposure at sub-apoptotic doses of ambient PM. Here, normal human bronchial epithelial BEAS-2B cells were acutely or repeatedly exposed to relatively low doses (5 $\mu g.cm^{-2}$) of FP ($PM_{2.5-0.18}$) or quasi-UFP (Q-UFP; $PM_{0.18}$) to better access the critical changes in mitochondrial morphology, functions, and dynamics. No significant cytotoxicity nor increase of apoptotic events were reported for any exposure. Mitochondrial membrane potential ($\Delta\Psi m$) and intracellular ATP content were also not significantly impaired. After cell exposure to sub-apoptotic doses of FP and notably Q-UFP, oxidative phosphorylation was increased as well as mitochondrial mass, resulting in increased production of mitochondrial superoxide anion. Given this oxidative boost, the NRF2-ARE signaling pathway was significantly activated. However, mitochondrial dynamic alterations in favor of accentuated fission process were observed, in particular after Q-UFP vs FP, and repeated vs acute exposure. Taken together, these results supported mitochondrial quality control and metabolism dysfunction as an early lung underlying mechanism of toxicity, thereby leading to accumulation of defective

mitochondria and enhanced endogenous ROS generation. Therefore, these features might play a key role in maintaining PM-induced oxidative stress and inflammation within lung cells, which could dramatically contribute to the exacerbation of inflammatory chronic lung diseases. The prospective findings of this work could also offer new insights into the physiopathology of lung toxicity, arguably initiate and/or exacerbate by acutely and rather repeated exposure to ambient FP and mostly Q-UFP.

KEYWORDS: Fine particles; Quasi-ultrafine particles; Normal human bronchial epithelial BEAS-2B cells; Toxicity; Mitochondrial function; Mitochondrial dynamics.

1 - INTRODUCTION

Epidemiological studies have highlighted associations between exposure to current and even high levels of ambient particulate matter (PM) and hospital admissions or mortality related to initiation and/or exacerbation of inflammatory lung diseases such as asthma and chronic obstructive pulmonary disease (COPD), and cancers (Atkinson et al. 2015; DeVries et al. 2017; Hamra et al. 2014; Heinrich and Schikowski 2018; Kim et al. 2017; Loomis et al. 2013; Mirabelli et al. 2016; Raaschou-Nielsen et al. 2013). Current health concerns are especially focused on fine particles (i.e., FP, with aerodynamic diameters smaller than 2.5 µm), notably due to their ability to migrate deeply and be retained in the respiratory tract. Recent studies drew special attention to the ultrafine particles (i.e., UFP, with aerodynamic diameters smaller than 0.1 µm), which are likely to be easily internalized in cells and to be more biologically reactive because of their high specific surface area (Stone et al. 2017). Due to the technologies required for their monitoring and their sampling, UFP have not yet been extensively studied and are currently not included in current air quality standards/guidelines although they possibly account for a large part of the adverse health effects triggered in humans by ambient PM.

While the role of ambient PM in initiating and/or exacerbating chronic inflammatory lung diseases has been reported, the various underlying mechanisms triggering airway inflammation are not yet well understood. Of course, all the intriguing signaling pathways sustaining the harmful cellular dysfunction are still far from being fully elucidated and are probably more complicated than originally expected. On the one hand, redox responses, inflammatory reactions, genetic and epigenetic alterations, and regulated cell death (RCD) are often considered as some of the main PM-induced cell outcomes (Abbas et al. 2009, 2010, 2013, 2016, 2019; Badran et al. 2020; Dergham et al. 2012, 2015; Garçon et al. 2006;

Gualtieri et al., 2010, 2011; Leclercq et al. 2016, 2017a, 2017b; Longhin et al. 2013, 2016; Saint-Georges et al. 2008, 2009; Platel et al., 2020; Sotty et al. 2019; Vales et al. 2015; Zhou et al. 2017). On the other hand, a growing number of studies suggested that mitochondria possibly play a key role in the pathogenesis of chronic inflammatory lung diseases and cancers (Lerner et al. 2016).

However, to date, only few authors have clearly mentioned mitochondrial dysfunction as a possible underlying mechanism involved in the PM-induced cell outcomes without going deeper into details other than apoptosis mechanism (Aggarwal et al. 2016; Ferecatu et al. 2010; Gualtieri et al. 2011; Jin et al. 2018; Kamdar et al. 2008; Liu et al. 2019; Upadhyay et al. 2003; Yang et al. 2018; Zheng et al. 2017). External stresses could actively disrupt sensitive mitochondrial functions by deregulating some critical processes in mitochondrial homeostasis, such as redox system, oxidative phosphorylation (OXPHOS), biogenesis, dynamics, and mitophagy (Lerner et al. 2016). Indeed, besides their fundamental role of energy supplier through OXPHOS, mitochondria are sensible sensors of early homeostatic disturbances related to nutrients and oxygen availability, intracellular calcium concentration, and cellular redox state. They are involved in many cell-signaling processes by generating reactive oxygen species (ROS), releasing damage-associated molecular patterns, and buffering calcium, thereby, actively coordinating the regulation of hypoxia and inflammation as well as apoptosis (Emerling et al. 2005; Meyer et al. 2018; Petrosillo et al. 2001; Schroedl et al. 2002; Zhou et al. 2011). Nevertheless, the nuclear factor erythroid 2 p45-related factor 2 (NRF2), as the well-known main key regulator of the cellular redox homeostasis, is well-equipped to counteract the mitochondrial redox response and therefore to maintain or recover the critical redox balance within the cell (Cho et al. 2015; Holmström et al. 2016; Jiang et al. 2017; Leclercq et al. 2018; Yue et al. 2016). Consequently, the mitochondrial dysfunction appears to be both a cause and a consequence of oxidative and/or inflammatory states of

airways in chronic inflammatory lung diseases such as asthma and COPD, or cancers (Bewley et al. 2017; Hara et al. 2018; Lerner et al. 2016; Reddy, 2011; Wiegman et al. 2015).

Because of their ability to monitor the redox environment in cell and regulate crucial survival processes, lung mitochondria are likely to be early targets of inhaled air pollutants, and to be involved in reported adverse health effects (Pardo et al. 2019). While mitochondria are often studied in the context of acute PM toxicity and consecutive apoptosis activation, only few toxicological studies have been interested in the adaptation mechanisms that may occur when exposing cells to more realistic sub-apoptotic doses of PM (Lavrich et al. 2018; Leclercq et al. 2018; Pardo et al. 2019). Recently, we reported for the first-time a mitochondrial stress, characterized by an increase of mitochondrial ROS production and a loss of membrane potential ($\Delta\Psi m$), in different human epithelial cell models repeatedly exposed to relatively low sub-apoptotic doses of FP. Interestingly, both the mitochondrial respiration and the ATP level were not significantly affected, thereby suggesting the occurrence of an adaptation mechanism that can efficiently compensate mitochondrial damage in order to maintain critical ATP production (Leclercq et al. 2018). However, at higher levels of FP, the NRF2-triggered antioxidant system failed to activate sufficient protection against the oxidative burst and the subsequent severe oxidative damage to critical cellular macromolecules (Leclercq et al. 2018).

Due to this wide spectrum of critical cellular functions that mitochondria are involved in, maintenance of a healthy population of mitochondria is also essential for cell survival (Zorov et al. 2019). As described by Scotland and Gottlieb (2015), impaired “mitochondrial quality control” results in accumulation of damaged mitochondria that may release more ROS, produce less ATP, have a lower threshold for cytochrome-c release resulting in apoptosis, undergo mitochondrial permeability transition pore (MPTP) opening resulting in cell death, or may release mitochondrial components (mtHSP60, oxidized mitochondrial

DNA) into cytosol, where its recognition by receptors for damage-associated molecular patterns activates inflammation. Mitochondrial turnover is therefore an integral aspect of quality control in which dysfunctional mitochondria are selectively eliminated through mitophagy and replaced through expansion of preexisting mitochondria (Zorov et al. 2019). Indeed, mitochondria are highly dynamic organelles undergoing coordinated cycles of fission and fusion, and mitochondrial trafficking, referred as “mitochondrial dynamics”, in order to maintain their shape, distribution and size. Their transient and rapid morphological adaptations are crucial for many cellular processes such as cell cycle, immunity, apoptosis and mitochondrial quality control (Tilokani et al. 2018). As reported by Dorn (2019), the four major protein mediators of mitochondrial dynamics are each members of the larger family of dynamin guanosine triphosphatases: mitofusins (MFN) 1 and 2, optic atrophy 1 (OPA1), and dynamin-related protein 1 (DRP1). MFN1, MFN2, and OPA1 are mitochondrial localized: MFN1 and MFN2 are inserted into the outer mitochondrial membrane (OMM) with both the amino and carboxy termini facing the cytosol, and OPA1 is localized to the inner mitochondrial membrane (IMM). DRP1 is almost entirely localized in the cytosol, until it is recruited to mitochondria where it binds to any of several OMM DRP1 receptor proteins.

Interestingly, for further insights into the results already publisher by Leclercq e al; (2018), we hypothesized that specific conditions leading to reduced NRF2 levels will drastically increase the adverse health effects of FP ($PM_{2.5\text{-}0.18}$) and possibly quasi-ultrafine particles (Q-UFP; $PM_{0.18}$). We investigated therefore the underlying mechanisms that govern the harmful effects of sub-apoptotic doses of the smallest size fractions of ambient PM on normal human bronchial epithelial BEAS-2B cells with respect to their toxicity, oxidative stress, and particularly mitochondrial function and dynamics. Taken together, the original results of this *in vitro* study should contribute to a better knowledge of the pro-survival mechanisms occurring in human bronchial epithelial cells exposed to ambient PM, and

provide new insights into the critical role of mitochondria in PM-induced chronic inflammatory airway diseases and even cancers.

2 - MATERIALS AND METHODS

2.1 - Reagents

BEAS-2B cells and all the chemical reagents were purchased from Sigma-Aldrich (Saint-Quentin Fallavier, France). MitoSOX™ Red mitochondrial superoxide indicator, Mitotracker® Green FM, Mitotracker® Red CMXROS, tetramethylrhodamine methyl ester perchlorate (TMRM), SYTOX® Red, SYTOX® Blue, DAPI slowfade® gold antifade, cell culture reagents, and molecular biology reagents were from Life Technologies (ThermoFisher Scientific, Villebon-sur-Yvette, France). CellTiter-Glo® luminescent cell viability, Caspase Glo® 3/7, Caspase Glo® 8, and Caspase Glo® 9 assays, and DeadEnd™ fluorometric TUNEL system were from Promega (Charbonnière-les-Bains, France). Nuclear extract and TransAM® NRF2 kits were from Active Motif (La Hulpe, Belgium). Cell Signaling Technology (Montigny-le-Bretonneux, France) provided rabbit polyclonal anti-human Phospho-DRP1 (Ser616) antibody (#3455), rabbit polyclonal anti human phospho-DRP1 (Ser637) antibody (#4867), and rabbit monoclonal anti-mouse IgG, HRP-linked antibody (S7076). Bio-Techne (Lille, France) provided mouse monoclonal anti-human actin antibody (MAB8929), mouse monoclonal anti-human HO-1/HMOX1/HSP32 antibody (GTS-1), mouse monoclonal anti-human NQO-1 antibody (A180), rabbit polyclonal anti-human TOMM20 antibody (NBP1-81556), mouse monoclonal anti-DRP1 antibody (3B5), rabbit monoclonal OPA1 antibody (1284B), mouse monoclonal anti-mitofusin 1 antibody (11E9-1H12), mouse monoclonal anti-mitofusin 2 antibody (4H8), and goat polyclonal anti-rabbit IgG, HRP-linked antibody (NB7160). Abcam plc (Cambridge, UK) provided rabbit polyclonal anti-human GCLM antibody (ab154017), rabbit polyclonal anti-VDAC1/Porin antibody - mitochondrial loading control (ab15895), total OXPHOS WB antibody cocktail (ab110413, which contains 5 mouse monoclonal antibodies, one each against CI-subunit

NDUFB8 (ab110242), CII-30kDa (ab14714), CIII-Core protein 2 (ab14745) CIV subunit I (ab14705), and CV alpha subunit (ab14748) as an optimized premixed cocktail). GeneTex, Inc. (Irvine, CA 92606 USA) provided mouse monoclonal anti-human FIS1 antibody (GT9810).

2.2 - Field campaign, sampling description, and physicochemical characterization of FP and Q-UFP

Both FP and Q-UFP sampling and physicochemical characterization have been already described in details by Saleh et al. (2018) and Sotty et al. (2019). Briefly, FP and Q-UFP were collected in Dunkerque, a highly industrialized coastal city, located in the north of France. Briefly, a high-volume impactor sampler has been set up to collect the fine fraction (i.e., $PM_{2.5\text{-}0.18}$, with aerodynamic diameters between 2.5 µm and 0.18 µm) by impaction, and quasi-ultrafine fraction (i.e., $PM_{0.18}$, with an aerodynamic diameter < 0.18 µm) by filtration on A4 sized-polycarbonate filters. Weekly samples were collected between September 9th, 2013 and April 14th, for 26 weeks in total, quickly stored at -20°C, and combined together after ultrasonic extraction in a Hanks' Balanced Salt Solution (HBSS; ThermoFisher Scientific). Size distribution and zeta potential were carried out by dynamic light scattering using zetasizer nano ZS (Malvern Panalytical, Orsay, France). After microwave mineralization under acid conditions, trace metal and metalloid concentrations of FP and Q-PUF were carried out by inductively coupled plasma mass spectrometry (NeXion 300x, Perkin Elmer, Waltham, MA, USA), as published elsewhere (Alleman et al. 2010, Mbengue et al. 2014). Before the analysis of surface contents by X-Ray photoelectron spectroscopy (XPS-K ALPHA, ThermoFisher Scientific), FP and Q-UFP were set up on silicon wafer, introduced in primary vacuum chamber (10^{-7} mbar, 60 min) to degas, and transferred in the analysis chamber (10^{-9} mbar, 320 min). Pressurized liquid extraction using a Dionex ASE 200

instrument (ThermoFisher Scientific) and preconcentration under a gentle stream of nitrogen in a TurboVap II water bath held at 60°C (Zymark, Roissy, France) were needed before analyzing PAH concentrations of FP and Q-UFP by high-pressure liquid chromatography (Waters 2695 Alliance system, on-line 996-photodiode array, and a 2475-fluorimetric detector; Waters SA, Saint-Quentin-en-Yvelines, France), as published elsewhere (Crenn et al. 2017).

2.3 - Cell culture and exposure strategies

The BEAS-2B cell line (ATCC CRL 9609™) was derived from normal human bronchial epithelial cells obtained from autopsy of non-cancerous individual. The culture conditions of BEAS-2B cells have been published by Leclercq et al. (2018). According to the future endpoints to study, BEAS-2B cells were seeded at the density of $30x10^3$ cells/well in 96 well white plates with clear bottom (Corning, ThermoFisher Scientific) and XF24 V7 microplates (Seahorse Bioscience, Billerica, MA, USA), at the density of $50x10^3$ cells/well in Nunc™ Lab-Tek™ II Chamber Slide™ 8 wells (ThermoFisher Scientific) or ibiTreat® culture chamber µSlides 8 wells (Ibidi Gmbh, Gräfelfing, Germany), and at the density of $200x10^3$ cells/well in CellBIND® 6-well microplates (Corning), using LHC-9 culture medium supplemented with 1% (v/v) amphotericin B (250 µg/mL) and 1% (v/v) penicillin (5,000 U/mL)/streptomycin (5,000 µg/mL) solution. BEAS-2B cells were thereafter incubated at 37°C for 24 h in a humidified atmosphere containing 5% CO_2. FP and Q-UFP stock solutions (2 µg/µL) were diluted in supplemented LHC-9 cell culture medium at 24 µg/mL to finally expose BEAS-2B cells at concentrations ranging from 0.5 to 50 µg/cm². Figure 1 depicts the global exposure strategy we applied to acutely or repeatedly expose BEAS-2B cells to FP or Q-UFP. BEAS-2B cells incubated thrice for 24 h to supplemented LHC-9 cell culture medium served as negative controls. For the acute exposure, BEAS-2B cells were incubated twice for

24 h to supplemented LHC-9 cell culture medium and, at last, for 24 h with supplemented LHC-9 cell culture medium with FP or Q-UFP. For repeated exposures, BEAS-2B cells were incubated thrice for 24 h to supplemented LHC-9 cell culture medium with FP or Q-UFP Just before each exposure, both FP and Q-UFP solutions were sonicated for 2 x 1 min. Except for the study of cytotoxicity, theoretical final doses of FP and Q-UFP applied on BEAS-2B cells were respectively 5 µg/cm² after a single exposure and 15 µg/cm² after the three repeated exposures. The rationale for selection of this dose (5 µg FP or Q-UFP/cm²/exposure) in the experimental strategy we applied was notably based the works published by Platel et al. (2020) and Sotty et al. (2019), reporting the harmful alterations of inflammatory, genetic and epigenetic endpoints in different human bronchial epithelial cell models, acutely and mostly repeatedly exposed to these relatively low cytotoxic doses of FP or Q-UFP. In addition, Leclercq et al. (2018) reported the harmful occurrence of mitochondrial dysfunction, as evidenced through severe mitochondrial ROS overproduction, $\Delta\Psi m$ loss, respiration reduction, and ATP inappropriate production, in BEAS-2B cells acutely and mostly repeatedly exposed to ambient FP at the sub-apoptotic dose of 10 µg/cm². In contrast, these authors indicated that a repeated exposure to relatively low doses of FP (2 µg/cm²) triggered a mitochondrial stress concurrently with some adaptation mechanisms that can contribute to maintain critical ATP production. Hence, as shown in the Results section of this publication, in order to suitably study the mitochondrial metabolism and/or dynamics, a particular attention has been paid to the verification that the exposure strategy we further applied ensure to limit the occurrence of massive regulated cell death and notably apoptosis in BEAS-2B cells after their exposure to FP or UFP. Immediately after the last exposure, adherent cells were washed once with 1mL-aliquots of cold sterile PBS, and either quickly prepared for microscopic observations and cytofluorometric analyses, or frozen at -80°C until the future analyses of the other toxicological endpoints under study.

264

265 **2.4 - Apoptosis**

266 Apoptosis within BEAS-2B cells acutely or repeatedly exposed to FP or Q-UFP was
267 evaluated through two complementary methods. Firstly, DNA fragmentation was evaluated
268 with Terminal deoxynucleotidyl transferase dUTP Nick End Labeling (TUNEL) technique,
269 using DeadEnd™ Fluorometric TUNEL system (Promega), a classic TdT-mediated dUTP
270 Nick-End Labeling (TUNEL) assay designed for the specific detection of apoptotic cells
271 within a cell population, according to the manufacturer's recommendations. Nucleus were
272 thereafter stained with DAPI slowfade® gold antifade (ThermoFisher Scientific). According
273 to supplier recommendations, BEAS-2B cells treated with DNase I (10 UI/mL, 30 min, 37°C)
274 served as positive controls. Fluorescent signals were observed with EVOS® FL imaging
275 system (Life Technologies). Secondly, caspase activities were measured using Caspase Glo®
276 3/7, Caspase Glo® 8, and Caspase Glo® 9 Assays (Promega) using a Spark® multimode
277 microplate reader (TECAN, Männedorf, Switzerland). BEAS-2B cells treated with hydrogen
278 peroxide (H_2O_2; 50 µM, 24 h, 37°C) served as positive control cells. Thirdly, fluorescence
279 labelling with SYTOX™ Red allowed to discriminate live cells among BEAS-2B cells acutely
280 or repeatedly exposed to FP or UFP. SYTOX™ Red is a high-affinity nucleic acid stain that
281 easily penetrates cells with compromised plasma membranes, but will not cross intact cell
282 membranes. After a brief incubation with SYTOX™ Red stain (λ excitation/emission
283 ~640/658 nm), the nucleic acids of dead cells fluoresce bright red when excited with 633 or
284 635 nm laser light. Cells were collected by a careful trypsinization, and after a recovering
285 time (30 min, 37°C, 5% CO_2), to avoid any artefact of cell detachment, stained with SYTOX™
286 red (5 nM, 10 min, 37°C, 5% CO_2; ThermoFisher Scientific). BEAS-2B cells treated with
287 menadione (100 µM, 4 h, 37°C, 5% CO_2) served as positive control cells. Fluorescent signals

were recorded on 50,000 cells using the Attune NxT flow cytometer (ThermoFisher Scientific).

2.5 - Intracellular ATP concentration

Intracellular ATP concentrations within BEAS-2B cells acutely or repeatedly exposed to FP or Q-UFP were determined immediately after their last exposure using CellTiter-Glo® luminescent cell viability assay (Promega). This assay system used the properties of a proprietary thermostable luciferase to enable reaction conditions that generate a stable "glow-type" luminescent signal. The mono-oxygenation of luciferin was catalyzed by luciferase in the presence of Mg^{2+}, ATP, and molecular oxygen, and resulted in the emission of light, directly linked to the ATP concentration and also the number of living cells. Luminescent signals were normalized with total protein concentration in each well with the Pierce™ BCA Protein Assay Kit (ThermoFisher Scientific).

2.6 - Mitochondrial membrane potential

Mitochondrial membrane potential ($\Delta\psi m$) was measured within BEAS-2B cells acutely or repeatedly exposed to FP or Q-UFP immediately after their last exposure. Cells were collected by a careful trypsinization, and after a recovering time (30 min, 37°C, 5% CO_2), to avoid any artefact of cell detachment, labelled with TMRM (25 nM, 30 min, 37°C, 5% CO_2; ThermoFisher Scientific). TMRM (λ excitation/emission ~488/570 nm) is a cell-permeant dye that accumulates in active mitochondria with intact membrane potentials. If the cells are healthy and have functioning mitochondria, the signal is bright. Upon loss of the mitochondrial membrane potential, TMRM accumulation ceases and the signal dims or disappears. Thereafter, after a wash with PBS, BEAS-2B cells were incubated with SYTOX® Blue (1 µM, 10 min, 37°C, 5% CO_2; ThermoFisher Scientific). SYTOX® Blue dead cell stain

(λ excitation/emission ~405/530 nm)) is a high-affinity nucleic acid stain that easily penetrates cells with compromised plasma membranes but will not cross uncompromised cell membranes. After brief incubation with SYTOX® Blue stain, the nucleic acids of dead cells fluoresce bright blue when excited with 405 nm violet laser light. BEAS-2B cells treated with FCCP (25 µM, 1 h, 37°C, 5% CO_2) to inhibit $\Delta\psi m$ served as positive control cells. Fluorescent signals were recorded on 50,000 cells using the Attune NxT flow cytometer (Thermofisher Scientific), and TMRM analyses were made only on negative SYTOX® Blue-cell population to specifically isolate only live BEAS-2B cells.

2.7 - Mitochondrial respiration

Oxygen consumption rates (OCR) were measured within BEAS-2B cells acutely or repeatedly exposed to FP or Q-UFP immediately after their last exposure using the XFe24 Extracellular Flux Analyzer (Agilent Technologies, Les Ulis, France). Briefly, supplemented LHC-9 cell culture medium with or without FP or Q-UFP were removed and BEAS-2B cells were washed once with Dulbecco′s Modified Eagle′s Medium (DMEM, Sigma-Aldrich), pH buffered at 7.35, supplemented with 10 mM glucose and 2 mM glutamine. Then, cells were incubated with DMEM in CO_2-free chamber at 37°C for 30 min. Baseline OCR was measured: (i) at the basal state, (ii) after oligomycin (Oli) injection (1 µM), (iii) after FCCP injection (i.e., first at 0.27 µM and then at 0.34 µM), and (iv) after rotenone (Rot)/antimycin A (AA) mix injection (0.5 µM). OCR measurements were normalized against cell densities. All data analyses were conducted with the Seahorse Wave software (Agilent technologies), and calculations of oxygen consumption due to proton leak (i.e., the respiration not modified by oligomycin), and ATP turnover (i.e. the respiration inhibited by oligomycin) were performed according to the method described by Divakaruni et al. (2014).

338 **2.8 - Superoxide anion production**

339 Superoxide anion production within live BEAS-2B cells acutely or repeatedly exposed
340 to FP or Q-UFP was evaluated using MitoSOX™ Red and MitoTracker® Green FM
341 (ThermoFischer Scientific). Firstly, to confirm mitochondrial localization of superoxide
342 production, immediately after their last exposure to FP or Q-UFP, cells seeded on Nunc™
343 Lab-Tek™ II Chamber Slide™ 8 wells (ThermoFisher Scientific) were washed once with
344 PBS and stained with MitoTracker® Green FM (70 nM, 30 min, 37°C, 5% CO_2) and
345 MitoSOX™ Red (5 µM, 30 min, 37°C, 5% CO_2) (ThermoFisher Scientific). The cell-permeant
346 MitoTracker® Green FM probe (λ excitation/emission ~490/516 nm) contains a mildly thiol-
347 reactive chloromethyl moiety for labeling mitochondria. MitoSOX™ Red mitochondrial
348 superoxide indicator (λ excitation/emission ~510/580 nm)) is a fluorogenic dye for highly
349 selective detection of superoxide in the mitochondria of live cells. MitoSOX™ Red reagent is
350 live-cell permeant and is rapidly and selectively targeted to the mitochondria. Once in the
351 mitochondria, MitoSOX™ Red reagent is readily oxidized by superoxide, but not by other
352 ROS- or reactive nitrogen species-generating systems, and exhibits red fluorescence.
353 Thereafter, Nunc™ Lab-Tek™ II Chamber Slide™ 8 wells were washed, mounted under
354 coverslip with DAPI slowfade® gold antifade mounting medium (ThermoFisher Scientific),
355 and thereafter observed with EVOS® FL imaging system (Life Technologies). The relative
356 quantification of fluorescence intensity of MitoSOX™ Red and MitoTracker® Green FM was
357 calculated using ImageJ software (https://imagej.nih.gov/ij/). Indeed, for each Nunc™ Lab-
358 Tek™ II Chamber Slide™ 8 wells, 3 fields were chosen at random per selected condition, and
359 for each of them, corrected total cell fluorescence (CTCF) of at least 10 cells was also
360 calculated as follows: integrated density – area of selected cell x mean fluorescence of
361 background). Secondly, BEAS-2B cells seeded in CellBIND® 6-well microplates (Corning)
362 were collected by a careful trypsinization, and after a recovering time (30 min, 37°C, 5%

CO_2), to avoid any artefact of cell detachment, labelled with MitoSOX™ Red (5 µM, 30 min, 37°C, 5% CO_2), and then, after washing with PBS, with SYTOX® Red (5 nM, 10 min, 37°C, 5% CO_2) (ThermoFsher Scientific). Fluorescent signals were recorded on 50,000 cells using the Attune NxT flow cytometer (Applied Biosystems, ThermoFisher Scientific). MitoSOX™ Red analyses were made only on negative SYTOX® Red population to specifically isolate only live BEAS-2B cells.

2.9 - NRF2 signaling pathway, and mitochondrial mass and dynamics

NRF2 binding activities were studied within BEAS-2B cells acutely or repeatedly exposed to FP or UFP using TransAM® NRF2 from Active Motif, according to the manufacturer's recommendations. Western blot analyses, performed on RIPA-extracts from exposed BEAS-2B cells using highly specific primary antibodies, allowed to investigate: (i) the antioxidant response through NRF2 signaling pathway activation: mouse monoclonal anti-human HO-1/HMOX1/HSP32 antibody-GTS-1, mouse monoclonal anti-human NQO-1 antibody-A180, and rabbit polyclonal anti-human GCLM antibody-ab154017), (ii) the mitochondrial mass: rabbit polyclonal anti-human TOMM20 antibody-NBP1-81556, rabbit polyclonal anti-VDAC1/Porin antibody-Mitochondrial Loading Control-ab15895, total OXPHOS WB antibody cocktail-ab110413, and (iii) the mitochondrial dynamics through the mitochondrial fission: mitochondrial fission rabbit polyclonal anti-human Phospho-DRP1 (Ser616) antibody-#3455, mouse monoclonal anti-human FIS-1 antibody-GT9810, and mouse monoclonal anti-DRP1 antibody-3B5, the mitochondrial fission inhibition: rabbit polyclonal anti-human phospho-DRP1 (Ser637) antibody-#4867, and the mitochondrial fusion: rabbit monoclonal OPA1 antibody-1284B, mouse monoclonal anti-mitofusin 1 antibody-11E9-1H12, and mouse monoclonal anti-mitofusin 2 antibody-4H8. Electrophoresis were realized with 20 µg total proteins on SDS-PAGE 4-12% bis-tris gels (Thermofisher Scientific). Then,

after transfer, nitrocellulose membranes were saturated in non-fat dry milk at 5% (v/v) in Tris-Buffer saline and TWEEN® 20 (0.1% v/v) solution (45 min, RT) and thereafter incubated with specific primary antibodies diluted according to the manufacturer's recommendations (overnight, 4°C). After three washes (5 min) in Tris-Buffer saline and TWEEN® 20 (0.1 v/v) solution, membranes were incubated with dedicated secondary antibodies: rabbit monoclonal anti-mouse IgG, HRP-linked antibody-S7076, goat polyclonal anti-rabbit IgG, HRP-linked antibody-NB7160 (1 h, RT). Finally, membranes were washed three times (5 min) and luminescent signals were read using ECL Advanced Western Blotting Detection reagent (GE Healthcare, Chicago, USA) on the Fusion FX Spectra (Vilbert-Lourmat, Marne la-Vallée, France). All the above-acquired signals were corrected with those of β-actin (mouse monoclonal anti-human actin antibody-MAB8929) or TOMM20 (rabbit polyclonal anti-human TOMM20 antibody-NBP1-81556).

2.10 - Live cell imaging of the mitochondrial dynamics

While mitochondria are highly dynamic organelles undergoing coordinated cycles of fission and fusion, and mitochondrial trafficking, referred as "mitochondrial dynamics", in order to maintain their shape, distribution and size, their transient and rapid morphological adaptations were observed using live cell imaging. Immediately after their last exposure to FP or Q-UFP, BEAS-2B cells seeded on ibiTreat® culture chamber µSlides 8 wells (Ibidi Gmbh), were washed once with PBS and stained with Mitotracker® Red CMXROS (250 nM, 30 min, 37°C, 5% CO_2) (ThermoFisher Scientific). The cell-permeant MitoTracker® Red CMXRos probe (λ excitation/emission ~579/599 nm) contains a mildly thiol-reactive chloromethyl moiety for labeling mitochondria. To label mitochondria, cells are simply incubated with MitoTracker® Red CMXRos probe, which passively diffuse across the plasma membrane and accumulate in active mitochondria. Cells were maintained at 37 °C and 5%

CO_2 during real time acquisitions. Time-lapse acquisitions were performed using an inverted Yokogawa Spinning Disk confocal microscope with a 63X oil-immersion lens (NA 1.4) (Zeiss, Jena, Germany). Images were acquired during 10 min and processed with ZEN software. All setups, using similar illumination and recording conditions (detector frequency, gain, and laser intensity), were applied between each condition.

2.11 - Transmission electron microscopy observations

Immediately after their last exposure, BEAS-2B cells acutely or repeatedly exposed to FP or Q-UFP were first fixed for 20 min with paraformaldehyde-glutaraldehyde (2% v/v) in PBS, and then fixed for 40 min by renewing the fixation solution. After a post-fixation with osmium tetroxide (1% v/v) in PBS, cells were progressively dehydrated in graded alcohols and embedded in an Epon/ethanol mixture and thereafter in Epon. After total polymerization, 85 nm sections were cut and stained with uranyl acetate (2% v/v) and Reynolds lead citrate prior to their observation in transmission electron microscopy (TEM; Zeiss EM900, Carl Zeiss SAS, Marly le Roi, France).

2.12 - Statistical analyses

Each experiment was repeated three times independently (n = 3). Data analyses and graphs were made with PRISM v7 software (Graph Pad, San Diego, USA). Data on graphs included means and standard deviations. Student's T-test was used to compare FP or Q-UFP-acutely or repeatedly exposed BEAS 2-B cell groups with control BEAS-2B cell groups. Significant differences were reported for p values <0.05.

3 - RESULTS

3.1 - Apoptosis within BEAS-2B cells exposed to FP or Q-UFP

The investigation of the adaptation mechanisms that may occur to counteract mitochondrial damages and preserve critical ATP production after BEAS-2B cell exposure to ambient FP or Q-UFP highly required to apply an original exposure strategy ensuring to observe some harmful cell effects without any massive RCD. Hence, the first step of this work aimed at confirming the absence of RCD, notably by apoptosis, within BEAS-2B cells acutely or repeatedly exposed to 5 µg/cm² doses of FP or Q-UFP. Acute (data not shown) as well as repeated (Figure 2-A) exposure of BEAS-2B cells to FP or Q-UFP did not trigger any significant DNA fragmentation. Moreover, neither FP nor Q-UFP exposure activated any initiator caspase-8 nor caspase-9, nor effector caspase 3/7 activity (Figure 2-B). In addition, for any exposure, no significant alteration of cell membrane selective permeability was detected by SYTOX® red analysis (Figure 2-C). Taken together, these results closely supported that acute and repeated exposures to 5 µg/cm² of FP or Q-UFP did not significantly trigger any significant cell death by apoptosis in BEAS-2B cells.

3.2 - Mitochondrial membrane potential and ATP concentration within BEAS-2B cells exposed to FP or Q-UFP

Mitochondrial membrane potential ($\Delta\psi m$) is generally consumed by ATP synthase to produce ATP. As shown in Figure 3-A, acute exposure to FP or Q-UFP did not significantly modify $\Delta\psi m$, whereas repeated exposure to these two PM size fractions were likely to slightly decreased $\Delta\psi m$, as indicated by TMRM immunofluorescence labelling. Accordingly, a similar profile of the intracellular ATP concentrations was reported within BEAS-2B cells acutely or repeatedly exposed to FP or Q-UFP, thereby supporting that these cells still

conserved their ability to produce ATP when exposed to both these particles at the dose of 5 µg/cm² (Figures 3-B and 3-C). Overall, these data clearly indicated that acute and repeated exposures to 5 µg/cm² of FP or Q-UFP did not significantly alter mitochondrial membrane potential nor ATP production in BEAS-2B cells.

3.3 - Mitochondrial respiration and mitochondrial mass within BEAS-2B cells exposed to FP or Q-UFP

As shown in Figure 4, there were statistically significant increases of OCR in BEAS-2B cells acutely or repeatedly exposed to FP or Q-UFP, without any major difference according to the PM size fraction nor the exposure strategy (Figures 4-A, 4-B, and 4-C and 4-D, respectively). In all cases, these increases of OCR were no longer seen after the administration of selective electron transport chain (ETC) inhibitors (rotenone, Rot/antimycin A, AA), thereby indicating that the increased respiration was specifically of mitochondrial origin (Figures 4-A and 4-B). Moreover, both the acute and the repeated exposures to FP or Q-UFP enhanced the maximum respiration, observed after FCCP administration, thus indicating the possible increase of the mitochondrial mass.

All the mitochondrial ETC complex subunits (CI subunit NDUFB8, CII-30kDa, CII-Core protein 2, CIV subunit I, and CV alpha subunit) and mitochondrial porins (translocase of outer mitochondrial membrane 20: TOMM20, and voltage dependent anion channel: VDAC) were also analyzed as mitochondrial mass markers (Figures 5-A, 5-B, 5-C, and 5-D, respectively). As shown in Figure 5-B, repeated exposure to FP as well as acute and repeated exposures to Q-UFP induced sharp increases of the CIV subunit I, as expressed vs β-ACTINE. In addition, the protein levels of all the complex subunits tend to increase with repeated exposure to both the PM size fractions, and especially Q-UFP. Moreover, as shown in Figure 5-C, there were significant increases of the CIV subunit I, as expressed vs

TOMM20, in BEAS-2B cells acutely or repeatedly exposed to FP or Q-UFP. Statistically significant decreases of CV-ATP5A, as expressed vs TOMM20, were reported in BEAS-2B cells acutely or repeatedly exposed to Q-UFP. As expected, VDAC and especially TOMM20 showed similar profiles of protein expression according to PM size fraction and exposure strategy, with statistically significant increases only within BEAS-2B repeatedly exposed to Q-UFP (Figure 5-D).

Overall, these results revealed that the increased mitochondrial respiration, mainly triggered by the repeated exposures to FP and mostly Q-UFP, was mainly accompanied by increases of the protein expression of CIV subunit I, and, only after the repeated exposure to Q-UFP, TOMM20 and VDAC mitochondrial porins.

3.4 - Superoxide anion production and NRF2 signaling pathway regulation within BEAS-2B cells exposed to FP or Q-UFP

The mitochondrial localization of the production of the superoxide anion, one of the ROS mainly originating from the OXPHOS process, was studied through a co-labeling of BEAS-2B cells with MitoTracker® Green FM and MitoSOX™ Red. The Figures 6-A indicates some increases of the MitoSOX™-related fluorescence within BEAS-2B cells repeatedly exposed to FP and mostly Q-UFP. Indeed, calculated CTCF for MitoSOX™ for BEAS-2B cells repeatedly exposed to FP (21.36 ± 2.98) and Q-UFP (26.97 ± 3.44) were significantly higher than those for control BEAS-2B cells (16.77 ± 2.73) ($p < 0.01$). Similar data were also reported in BEAS-2B cells after acute exposure to Q-UFP (data not shown). Moreover, both the Figures 6-B and 6-C showed that acute exposure to UFP, on the one hand, and repeated exposure to FP and mostly Q-UFP, on the other hand, induced a significant overproduction of the superoxide anion in BEAS-2B cells. Moreover, NRF2 signaling pathway was significantly activated (Figures 7-A, 7-B, 7-C, 7-D, and 7-E). However, there

were statistically significant increases of NRF2 binding activity in BEAS-2B cells only after their acute exposures to FP and Q-UFP (Figure 7-A). Nevertheless, the protein expressions of the downstream antioxidant effectors, such as NADPH quinone oxydoreductase 1 (NQO-1), heme oxygenase-1 (HO-1), and glutamate cysteine ligase modifier subunit (GCLM), were further increased after the repeated exposure to FP and the acute and mostly repeated exposures to Q-UFP (Figures 7-C, 7-D, and 7-E, respectively). As a whole, these results supported the ROS overproduction in BEAS-2B cells acutely and mostly repeatedly exposed to FP, and at the higher extend, Q-UFP.

3.5 - Mitochondrial dynamics within BEAS-2B cells exposed to FP or Q-UFP

OPA-1 and mitofusins (MFN-1, MFN-2), as effector proteins of mitochondrial fusion, are involved in the fusion of OMM and IMM, respectively. As shown in Figures 8-A and 8-B, BEAS-2B cell exposure to FP or Q-UFP did not significantly modify any protein expression both the mitofusins. Only a slight but significant increase of the OPA-1 protein expression was seen in BEAS-2B cells after their repeated exposure to Q-UFP (Figure 8-B). Conversely, the mitochondrial fission 1 protein (FIS-1) and dynamin-related protein (DRP1) are involved in mitochondrial fission. The accumulation of FIS-1 on OMM allows the recruitment of the cytoplasmic protein DRP1 to trigger fission process, and the phosphorylation of DRP1 on serine 616 (S616) is known to stimulate mitochondrial fission while its phosphorylation on serine 637 (S637) inhibits it. As shown in Figures 8-C and 8-D, acute and mostly repeated exposures to FP and particularly Q-UFP triggered significant increases of DRP1 and/or P-DRP1 (S616) protein expression without any significant change of P-DRP1 (S637) protein expression in BEAS-2B cells. There was a clear trend of overexpression of FIS-1 protein expression, despite relatively high inter-experiment variability; however, a statistically significant increase of this key parameter was reported only after their repeated exposure to

Q-UFP. Figure 8-E, showing live BEAS-2B cells labeled with MitoTracker® Red, supported the above-noticed alteration of the mitochondrial dynamics through the reduction of the coordinated cycles of fission and fusion, and mitochondrial trafficking, after their repeated exposure to FP and rather Q-UFP.

As shown in Figure 9, TEM observations of fixed BEAS-2B cells repeatedly exposed to Q-UFP clearly showed the absence of any apparent toxicity, as compared to control BEAS-2B cells. In control BEAS-2B cells, mitochondria were heterogeneous in shape, rounded or elongated, with numerous cristae. IMM and OMM appeared intact and the matrix integrity was fully preserved. Like negative control cells, there were no marked mitochondrial abnormalities in Q-UFP-repeatedly exposed BEAS-2B cells, also characterized by the absence of swollen mitochondria with disarrangement and distortion of cristae, and the apparent integrity of the OMM.

However, time-lapse video microscopy of live BEAS-2B cells repeatedly exposed to FP or Q-UFP provided relevant real time imaging of their mitochondrial dynamics, after their immunofluorescence labelling with MitoTracker® Red (Figure 10). Indeed, the reduction of the mitochondrial dynamics in BEAS-2B cells repeatedly exposed to FP and mostly Q-UFP, was noticed. Indeed, as shown in the two series of photos of the control BEAS-2B cells, some modifications of the mitochondrial network can be seen after 6 s of observation by comparing the photos chronologically to each other (see also Figure 10-A, photo areas with white dotted lines). Some fragments of the mitochondrial network, originally separated after 1 s of observation seemed also to be fused after 6 s of observation. However, such mitochondrial dynamics were not reported in BEAS-2B cells after their repeated exposures to FP or Q-UFP. As a matter of fact, after 6 s of observation, the comparison of the photos chronologically to each other (see also the photo areas with white dotted lines) revealed that some fragments of the mitochondrial network, originally separated after 1 s of observation were still clearly

distinct after 6 s of observation. The difference of the mitochondrial dynamics within BEAS-2B cells repeatedly exposed to FP or Q-UFP and those of control BEAS-2B cells was easily visible and recognizable in the videos supplied as supplemental data. As shown by the photo series, and mostly by the videos (see also supplemental data), in repeatedly-exposed BEAS-2B cells to FP and mostly UFP, only a small part of mitochondria was also transported over significant distances during a given observation time, while others were in the state of relative rest, as compared to control BEAS-2B cells.

4 - DISCUSSION

To better study the possible occurrence of the underlying adaptation mechanisms that can efficiently compensate mitochondrial damages, human bronchial epithelial BEAS-2B cells were both acutely or repeatedly exposed to relatively low doses (i.e., 5 µg/cm²) of ambient FP or Q-UFP. Indeed, the dose we applied was among the lowest reported in the literature to give harmful effects whilst limiting a massive cell death (Boublil et al. 2013; Gualtieri et al. 2010, 2011, 2018; Leclercq et al. 2016, 2017, 2018; Longhin et al. 2013, 2016, 2019; Platel et al; 2019; Sotty et al. 2019). The analysis of several cell death markers, such as DNA fragmentation, caspase activation, and membrane permeability, supported the absence of substantial cytotoxicity, notably by apoptosis, in BEAS-2B cells for each exposure protocol. Neither $\Delta\Psi m$ nor intracellular ATP concentration were significantly altered in BEAS-2B cells repeatedly exposed to both the PM size fractions, thereby supporting the avoidance of massive cell toxicity. In contrast to other studies, the exposure strategy we developed ensured the maintenance of cell conditions devoted to trigger the adaptation and/or survival underlying mechanisms, studying mitochondrial function rather than RCD (Kamdar et al. 2008; Jin et al. 2018; Wang et al 2019).

We reported here significant increases of the mitochondrial function, as studied by OCR, specifically from mitochondrial origin, in BEAS-2B cells acutely and mostly repeatedly exposed to FP or Q-UFP, together with equivalent increases in maximal respiration. Accordingly, Lavrich et al. (2018) reported an increased OCR within BEAS-2B cells exposed to low dose of 1,2-naphthoquinone, a PAH systematically found within ambient PM. However, this increase of OCR was no longer observed in isolated mitochondria no when normalizing results to the mitochondrial mass. An increase of the non-mitochondrial respiration that can be related to a possible increase of mitochondrial mass rather than the

593 spare capacity consumption was also suggested. To test this hypothesis, some classical
594 mitochondrial mass markers, such as ETC complex subunits and mitochondrial porins were
595 studied, and, as anticipated, we supported that the increases of mitochondrial OCR noticed
596 after repeated exposure to FP, and mostly Q-UFP, were accompanied by those of ETC
597 complex subunits. Whether it is expressed vs β-ACTIN or specifically vs TOMM20, the
598 relative protein intensity of CIV-MTCO1 subunit, where dioxygen is consumed, was
599 increased after repeated exposure to FP and particularly after acute and mostly repeated
600 exposure to Q-UFP. Moreover, when expressed vs TOMM20, the relative protein intensity of
601 CV-ATP5A subunit, also called mitochondrial ATPase, revealed a certain tendency towards a
602 reduction in BEAS-2B cells repeatedly exposed to FP, but a significant reduction in those
603 acutely or repeatedly exposed to Q-UFP. Increasing trends in BEAS-2B cells repeatedly
604 exposed to FP or acutely exposed to Q-UFP, but significant increases in those repeatedly
605 exposed to Q-UFP, were found when studying the VDAC and TOMM20 mitochondrial
606 porins. All together, these findings supported that changes of the mitochondrial respiration,
607 mainly triggered by the repeated exposure to FP or rather UFP, were accompanied by changes
608 of some mitochondrial ETC complexes and porins. Likewise, Hoffman et al. (2013), in their
609 study about the long-term effects of cigarette smoking on BEAS-2B cells, described similar
610 ETC complexes after 6-month exposure. In other studies, Wang et al. (2019) reported a dose-
611 dependent increase in CIV by exposing the popular SH-SY5Y neuroblastoma cells to ambient
612 FP and Guo et al. (2017) noted that exposure to ambient FP induced decreases in the activities
613 of several ATPases in rat nasal mucosa. Accordingly, these results may indicate an adaptive
614 rise in cellular energy demand to better eliminate damage to the different cellular components,
615 or to compensate oxidative damage to mtDNA (Winckelmans et al. 2017; Xu et al. 2018).
616 However, and somewhat interestingly, the exposure to higher doses of ambient PM, although
617 non-cytotoxic, was reported as decreasing mitochondrial oxygen consumption, as well as

618 complex enzymatic activity, thereby possibly exceeding the mitochondrial adaptation
619 mechanisms (Leclercq et al. 2018; Malinska et al. 2018; Pardo et al. 2017; Karoui et al. 2019).
620 Along with inflammation, oxidative stress is frequently considered to be the primary
621 critical underlying mechanism dramatically induced by ambient PM (Abbas et al. 2010, 2013,
622 2016, 2019; Billet et al. 2007, 2008; Bocchi et al. 2016; Dergham et al. 2012, 2015; Garçon et
623 al. 2006; Gualtieri et al. 2010, 2011; Halonen et al. 2015; Leclercq et al. 2016, 2017b, 2018;
624 Longhin et al. 2013, 2016, Sotty et al. 2019). Accordingly, in this work, acute exposure to Q-
625 UFP as well as, to a higher extent, repeated exposure to FP and mostly Q-UFP, triggered
626 increases of superoxide anion production by mitochondria. This oxidative boost was
627 associated with NRF-2 signaling pathway activation. Because of its key role as master
628 regulator of the cell redox homeostasis, NRF-2 is also well-equipped to counteract ROS
629 production and is critical for maintaining the redox balance in the cell (Wardyn et al. 2015).
630 Following exposure to oxidants or electrophiles, NRF2 accumulates in the nucleus where it
631 binds to antioxidant response element (ARE) in the upstream regulatory regions of genes
632 encoding NRF-2 targets, including antioxidant enzymes, proteins involved in the metabolism
633 and clearance of toxicants, protection against metal toxicity, inhibition of inflammation, repair
634 and removal of damaged proteins, as well as other transcription and growth factors (Suzuki et
635 al. 2016). However, there were some discrepancies in this study between the NRF-2 binding
636 activities to ARE sequences and the protein expression of some associated antioxidant
637 enzymes (i.e. HO-1, NQO1, GCLM) after repeated exposure to both the PM size fractions.
638 Accordingly, Leclercq et al. (2018), studying the NRF2 signaling pathway activation within
639 BEAS-2B cells repeatedly exposed to ambient FP, reported a relatively low activation of the
640 NRF2 transcription factor in cells repeatedly exposed to the highest dose of FP, thereby
641 suggesting NRF2 relocalization, binding inactivation, or degradation even under a noticeable
642 oxidative stress. While NRF-2 signaling pathway is known to be activated in lung cells in

643 case of relatively low level of oxidative stress, it has been shown to be inhibited following
644 higher stress level. Our results might be explained by an inhibition of NRF-2 response after
645 repeated exposures to PM and a delayed lag between NRF-2 transcriptional activity regulation
646 and downstream protein degradation. Kovac et al. (2015), aiming to provide a detailed
647 analysis of the interaction between ROS and the NRF2 signaling pathway, indicated that the
648 NRF2 activity affects ROS production via mitochondria. Moreover, Boutten et al. (2011) and
649 Vucic et al. (2014) indicated that the NRF2-mediated antioxidant pathway was altered at
650 multiple levels in COPD bronchial airways leading to an important redox imbalance.
651 Recently, it has emerged that one of the important functions of NRF2 is to modulate
652 mitochondrial function (Holmström et al. 2016). Hence, in this work, the partial uncoupling
653 between the superoxide anion production and the NRF2 signaling pathway activation after the
654 repeated exposure to FP and mostly Q-UFP could dramatically contribute to mitochondrial
655 ROS overproduction and possibly to mitochondrial metabolism disruption.

656 It is noteworthy that the increases of the mitochondrial mass noticed in the present study
657 seemed to be closely consistent with the above-described NRF2 signaling pathway activation,
658 since the peroxisome proliferator-activated receptor gamma coactivator (PGC1-α), a major
659 regulator of mitochondrial biogenesis, is known to induce NRF2 gene transcription (Chen et
660 al. 2011; Wu et al. 1999). In cooperation with NRF2, PGC1-α also stimulates nuclear
661 respiratory factor-1 (NRF1) activity, another transcription factor leading to the expression of
662 some of the genes clearly involved into the mitochondrial biogenesis and maintenance, such
663 as *mitochondrial transcription factors A* and *B* (Kelly and Scarpulla, 2004; Scarpulla, 2008).
664 While ARE sequences are present on the *NRF1* promotor, *NRF2* activation may therefore
665 promote mitochondrial biogenesis through *NRF1* transcription (Piantadosi et al. 2008).

666 Depending on the energy substrate availability, energy demands or redox state, the cell
667 may increase or decrease the number and size of mitochondria, and altered copy number by

damage can result in mitochondrial dysfunction (Chao and Kleeberger, 2019). Indeed, mitochondria, which form a dynamic interconnected intracellular network, are highly dynamic organelles undergoing coordinated cycles of fission/fusion, and mitochondrial trafficking, also referred as “mitochondrial dynamics”, in order to maintain their shape, distribution and size according to the metabolic needs of the cell (Tilokani et al. 2018). Mitochondria undergo membrane remodeling through cycles of fusion and division; the balance of these processes controls the mitochondrial structure and metabolism as well as the cell cycle and results in the intermixing of the mitochondrial population in the cell both during normal mitochondrial turnover in homeostatic physiology and in response to mitochondrial or cellular stress. Increased fusion and/or reduced fission promote the formation of elongated mitochondrial networks to maintain membrane potential, whereas increased fission and/or reduced fusion cause mitochondrial fragmentation to eliminate defective mitochondria by mitophagy or to generate new organites from fissioned mitochondria. Mitochondrial fusion and fission cycle are essential for numerous cell processes including mitosis, cell immunity and mitochondrial quality control (Chan et al. 2019; Cloonan and Choi, 2016; Tilokani et al. 2018; Youle et al. 2012; Zorov et al. 2019). In BEAS-2B cells repeatedly exposed to FP and markedly Q-UFP, a slight increasing trend in the expression of fusion markers and a significant increase of OPA-1 in BEAS-2B cells repeatedly exposed to UFP were noticed. However, this increase might mainly result from increased mitochondrial mass given the localization of these proteins on mitochondrial membrane. By contrast, acute and mostly repeated exposure to FP and especially to Q-UFP triggered increases of FIS1 and DRP1 fission proteins, with an accentuated effect in BEAS-2B cells repeatedly exposed. Moreover, DRP1 activation was further highlighted by its phosphorylation at serine 616. Similar increases, all at once, of fusion and fission markers (i.e., OPA1 and FIS1, and MFN1, MFN2, and DRP1, respectively) were also described in

693 BEAS-2B cells treated with cigarette smoke exhaust, in SH-SY5Y cells treated with FP, and
694 in rats treated with FP (Guo et al. 2017; Hoffmann et al. 2013; Li et al. 2015; Wang et al.
695 2019). These modifications are sometimes associated with ultrastructural changes, which can
696 include mitochondria swelling, disruption of mitochondrial cristae, and loss of mitochondrial
697 density (Guo et al. 2017; Leclercq et al. 2018; Li et al. 2013, 2015). Because of their quasi-
698 nanometric size, Q-UFP are more likely to be internalized within lung tissues and cells, and
699 potentially interact with mitochondria, than FP. Li et al. (2013) reported a higher
700 internalization of UFP in mitochondria of BEAS-2B cells compared to those of FP. However,
701 other studies, including ours, did not clearly observed mitochondrial internalization of Q-
702 UFP, thereby supporting the influence of physicochemical characteristics and doses applied
703 on the different cell models on their capacity to be internalized and visualized into
704 mitochondria.

705 However, despite the lack of morphological mitochondrial alterations reported in fixed
706 BEAS-2B cells, time-lapse video microscopy of live BEAS-2B cells acutely or repeatedly
707 exposed to FP or mostly Q-UFP provided relevant real time imaging of the alteration of the
708 mitochondrial dynamics, through the reduction of the coordinated cycles of fission/fusion,
709 and mitochondrial trafficking, Indeed, in repeatedly-exposed BEAS-2B cells to FP and mostly
710 UFP, only a small part of mitochondria was also transported over significant distances, while
711 others were in the state of relative rest, as compared to control cells. The relevant alteration of
712 the mitochondrial dynamics we emphasized in this work closely agreed with those already
713 noticed in other *in vitro* and *in vivo* models exposed to cigarette smoke exhaust and ambient
714 PM (Guo et al. 2017; Hoffmann et al. 2013; Li et al. 2015; Wang et al. 2019). According to
715 the ROS overproduction already noticed within BEAS-2B cells acutely and mostly repeatedly
716 exposed to FP and Q-UFP, to a higher extent, accumulating evidence suggested that cellular
717 and mitochondrial redox homeostasis is linked to mitochondrial dynamics in a cell- and

718 tissue-dependent manner (Willems et al. 2015). ROS (over)production also regulated
719 mitochondrial dynamics through acting on mitochondrial fusion and fission proteins, thereby
720 permitting (auto)regulation of mitochondrial morphology and function by redox-mediated
721 signaling.

722 Before concluding, it is highly important to emphasize that, in this work, BEAS-2B
723 cells were acutely or repeatedly exposed to FP and Q-UFP, instead of UFP. All the above-
724 reported results about the Q-PUF-induced underlying mechanisms of toxicity, and notably
725 mitochondrial function and dynamics alterations, cannot be directly extrapolated to UFP.
726 Stone et al. (2018) reviewed in detail a rather large mechanistic body of research to better
727 clarify the relationships between these mechanistic endpoints and the physicochemical
728 characteristics of nanomaterials and UFP, vs PM. The critical role of their physicochemical
729 characteristics regarding their toxicity, including factors in addition to size and surface area,
730 such as solubility, charge, chemical and biological composition, coating, and
731 agglomeration/aggregation, was also strongly highlighted. This information is, therefore,
732 important because it means that not Q-PUF and PUF have exactly the same potential to
733 dramatically interact with cellular and molecular critical targets within cells in the same way
734 and with the same harmful health effects.

735 Taken together, these results demonstrated the ability of FP and mostly Q-UFP to
736 trigger some alterations of the mitochondrial function and dynamics at non-apoptotic stage,
737 thereby highlighting mitochondria as early critical targets of the smallest size fractions of the
738 ambient PM. Indeed, exposure to both PM size fractions increased mitochondrial OCR as
739 well as mitochondrial mass without modifying global $\Delta\Psi m$ nor mitochondrial ATP
740 concentration. As a consequence, dynamic modifications in favor of accentuated fission
741 process were observed, in particular after Q-UFP vs FP, and repeated vs acute exposures.
742 Overall, the prospective findings of this work could offer new insights into the

743 pathophysiology of lung toxicity, arguably initiate and/or exacerbate by acutely and rather
744 repeated exposure to ambient FP and mostly Q-UFP. Given their important biological
745 reactivity, the effective monitoring of ambient Q-UFP and their integration within air quality
746 standards should be urgently consider in order to significantly contribute to reduce the
747 dramatic health impact of ambient air pollution.
748

5 - FUNDINGS

The research described in this article benefited from grants from the Hauts-de-France Region Council (Convention n°13004366). The EA4483-IMPact de l'Environnement Chimique sur la Santé (IMPECS) of the Lille University participates in the CLIMIBIO project, which is financially supported by the Hauts-de-France Region Council, the French Ministry of Higher Education and Research, and the European Regional Development Funds. JS received a PhD fellowship funded by Lille University.

6 - REFERENCES

Abbas I, Saint-Georges F, Billet S, Verdin A, Mulliez P, Shirali P, Garçon G (2009) Air pollution Particulate Matter ($PM_{2,5}$)-induced gene expression of volatile organic compound and/or polycyclic aromatic hydrocarbon-metabolizing enzymes in an in vitro coculture lung model. Toxicol In vitro 2:37-46.

Abbas I, Garçon G, Saint-Georges F, Billet S, Verdin A, Gosset P, Mulliez P, Shirali P (2010) Occurrence of molecular abnormalities of cell cycle in L132 cells after *in vitro* short-term exposure to air pollution $PM_{2,5.}$ Chem Biol Interact 188:558-565.

Abbas I, Garçon G, Saint-Georges F, André V, Gosset P, Billet S, Le Goff J, Verdin A, Mulliez P, Sichel F, Shirali P (2013) Polycyclic aromatic hydrocarbons within airborne particulate matter ($PM_{2,5}$) produced DNA bulky stable adducts in a human lung cell coculture model. J Appl Toxicol 33:109-119.

Abbas I, Verdin A, Escande F, Saint-Georges F, Cazier F, Mulliez P, Courcot D, Shirali P, Gosset P, Garçon G (2016) In vitro short-term exposure to air pollution $PM_{2,5-0,3}$ induced cell cycle alterations and genetic instability in a human lung cell coculture model. Env Res 147:146-158.

Abbas I, Badran G, Verdin A, Ledoux F, Roumie M, Lo Guidice JM, Courcot D, Garçon G. (2019) In vitro evaluation of organic extractable matter from ambient $PM_{2.5}$ using human bronchial epithelial BEAS-2B cells: Cytotoxicity, oxidative stress, pro-inflammatory response, genotoxicity, and cell cycle deregulation. Environ Res. 171:510-522.

Aggarwal S, Mannam P, Zhang J (2016) Differential regulation of autophagy and mitophagy in pulmonary diseases. Am J Physiol Lung Cell Mol Physiol 311:L433-L452.

781 Alleman LY, Lamaison L, Perdrix E, Robache A, Galloo J-C (2010) PM_{10} metal
782 concentrations and source identification using positive matrix factorization and wind
783 sectoring in a French industrial zone. Atmospheric Research 96:612-625.
784 Atkinson RW, Carey IM, Kent AJ, Van Staa TP, Anderson HR, Cook DG (2015) Long-term
785 exposure to outdoor air pollution and the incidence of chronic obstructive pulmonary
786 disease in a national English cohort. Occup Environ Med 72(1):42-48.
787 Badran G, Ledoux F, Verdin A, Abbas I, Roumie M, Genevray P, Landkocz Y, Lo Guidice
788 JM, Garçon G, Courcot D. (2020). Toxicity of fine and quasi-ultrafine particles: focus on
789 the effects of organic extractable and non-extractable matter fractions. Chemosphere
790 243:125440.
791 Beelen R, Raaschou-Nielsen O, Stafoggia M (2013) Effects of long-term exposure to air
792 pollution on natural-cause mortality: an analysis of 22 European cohorts within the
793 multicentre ESCAPE project. The lancet 383:785-795.
794 Bewley MA, Preston JA, Mohasin M, Marriott HM, Budd RC, Swales J, Collini P, Greaves
795 DR, Craig RW, Brightling CE, Donnelly LE, Barnes PJ, Singh D, Shapiro SD, Whyte
796 MKB, Dockrell DH (2017) Impaired Mitochondrial Microbicidal Responses in Chronic
797 obstructive Pulmonary Disease Macrophages. Am J Respir Crit Care Med 196(7):845-855.
798 Billet S, Garçon G, Dagher Z, Verdin A, Ledoux F, Cazier F, Courcot D, Aboukais A, Shirali
799 P (2007) Ambient particulate matter ($PM_{2.5}$): physicochemical characterization and
800 metabolic activation of the organic fraction in human lung epithelial cells (A549). Environ.
801 Res. 105:212-223.
802 Billet S, Abbas I, Le Goff J, Verdin A, Andre V, Lafargue P, Garçon G (2008) Genotoxic
803 potential of polycyclic aromatic hydrocarbons-coated onto airborne particulate matter
804 ($PM_{2.5}$) in human lung epithelial A549 cells. Cancer Lett. 270:144-155.

805 Bocchi C, Bazzini C, Fontana F, Pinto G, Martino A, Cassoni F. (2016) Characterization of
806 urban aerosol: seasonal variation of mutagenicity and genotoxicity of $PM_{2.5}$, PM_1 and
807 semi-volatile organic compounds. Mutat Res. 809:16-23.
808 Boublil L, Assémat E, Borot M,C, Boland S, Martinon L, Sciare J, Baeza-Squiban A (2013)
809 Development of a repeated exposure protocol of human bronchial epithelium *in vitro* to
810 study the long-term effects of atmospheric particles. Toxicol in vitro 27:533-542.
811 Boutten A, Goven D, Artaud-Macari E, Boczkowski J, Bonay M (2011) NRF2 targeting: a
812 promising therapeutic strategy in chronic obstructive pulmonary disease. Trends Mol Med
813 17(7):363-371.
814 Chen J, Dai AG, Fu MJ, Long ZG, Zhu LM (2011) The roles of PPAR-gamma/PGC-1alpha
815 to Nrf2/gamma-GCS-h in lung of guinea pigs with bronchial asthma. Chinese journal of
816 applied physiology 27(2):225-229.
817 Cho HJ, Kleeberger SR (2015) Association of Nrf2 with airway pathogenesis: lessons learned
818 from genetic mouse models. Arch Toxicol 89:1931-1957.
819 Cloonan SM, Choi AM (2016) Mitochondria in lung disease. J Clin Invest. 126(3):809-820.
820 Crenn V, Chakraborty A, Fronval I, Petitprez D, Riffault V (2018) Fine particles sampled at
821 an urban background site and an industrialized coastal site in Northern France—Part 2:
822 Comparison of offline and online analyses for carbonaceous aerosols. Aerosol Science and
823 Technology 52:287-299.
824 Dergham M, Lepers C, Verdin A, Billet S, Cazier F, Courcot D, Shirali P, Garçon G (2012)
825 Prooxidant and proinflammatory potency of air pollution particulate matter ($PM_{0,3-2,5}$)
826 produced in rural- urban- or industrial surroundings in human bronchial epithelial cells
827 (BEAS-2B). Chem Res Toxicol 25:904-919.
828 Dergham M, Lepers C, Verdin A, Billet S, Cazier F, Courcot D, Shirali P, Garçon G (2015)
829 Temporal-spatial variations of the physicochemical characteristics of air pollution

particulate matter ($PM_{0,3-2,5}$) and toxicological effects in human bronchial epithelial cells BEAS-2B. Env Res 137:256-267.

DeVries R, Kriebel D, Sama S (2017) Outdoor Air Pollution and COPD-Related Emergency Department Visits, Hospital Admissions, and Mortality: A Meta-Analysis. COPD 14(1):13-121.

Divakaruni AS, Paradyse A, Ferrick DA, Murphy AN, Jastroch M (2014) Analysis and Interpretation of Microplate-Based Oxygen Consumption and pH Data. Methods in Enzymology 547:309-354.

Dorn GW 2nd. (2019) Evolving Concepts of Mitochondrial Dynamics. Annu Rev Physiol. 81:1-17.

Emerling BM, Platanias LC, Black E, Nebreda AR, Davis RJ, Chandel NS. (2005) Mitochondrial reactive oxygen species activation of p38 mitogen-activated protein kinase is required for hypoxia signaling. Mol Cell Biol. 25(12):4853-4862.

Ferecatu I, Borot MC, Bossard C, Leroux M, Boggetto N, Marano F, Baeza-Squiban A, Andreau K (2010) Polycyclic aromatic hydrocarbon components contribute to the mitochondria-antiapoptotic effect of fine particulate matter on human bronchial epithelial cells via the aryl hydrocarbon receptor. Part Fibre Toxicol 7:1-14.

Garçon G, Dagher Z, Zerimech F, Ledoux F, Courcot D, Aboukais A, Puskaric E, Shirali P (2006) Dunkerque city air pollution particulate matter-induced cytotoxicity, oxidative stress and inflammation in human epithelial lung cells (L132) in culture. Toxicol *in vitro* 20:519-528.

Gualtieri M, Øvrevik J, Holme JA, Perrone MG, Bolzacchini E, Schwarze PE, Camatini M (2010) Differences in cytotoxicity versus pro-inflammatory potency of different PM fractions in human epithelial lung cells, Toxicol *in vitro* 24:29-39.

Gualtieri M, Ovrevik J, Mollerup S, Asare N, Longhin E, Dahlman HJ, Camatini M, Holme JA (2011) Airborne urban particles (Milan winter-$PM_{2,5}$) cause mitotic arrest and cell death: Effects on DNA mitochondria AhR binding and spindle organization. Mutat Res 713:18-31.

Guo Z, Hong Z, Dong W, Deng C, Zhao R, Xu J, Zhuang G, Zhang R. (2017) $PM_{2.5}$-induced oxidative stress and mitochondrial damage in the nasal mucosa of rats. Int J Environ Res Public Health. 29: 14(2).

Guo C, Zhang Z, Lau AKH, Lin CQ, Chuang YC, Chan J, Jiang WK, Tam T, Yeoh EK, Chan TC, Chang LY, Lao XQ (2018) Effect of long-term exposure to fine particulate matter on lung function decline and risk of chronic obstructive pulmonary disease in Taiwan: a longitudinal, cohort study. Lancet Planet Health 2(3):114-125.

Halonen JI, Hansell AL, Gulliver J, Morley D, Blangiardo M, Fecht D, Toledano MB, Beevers SD, Anderson HR, Kelly FJ, Tonne C (2015) Road traffic noise is associated with increased cardiovascular morbidity and mortality and all-cause mortality in London. Eur Heart J. 36(39):2653-2661.

Hamra GB, Guha N, Cohen A, Laden F, Raaschou-Nielsen O, Samet JM, Vineis P, Forastiere F, Saldiva P, Yorifuji T, Loomis D (2014) Outdoor particulate matter exposure and lung cancer: a systematic review and meta-analysis. Environ Health Perspect 122:906-911.

Hara H, Kuwano K, Araya J (2018) Mitochondrial Quality Control in COPD and IPF. Cells 7(8):86.

Heinrich J, Schikowski T (2018) COPD Patients as Vulnerable Subpopulation for Exposure to Ambient Air Pollution. Curr Environ Health Rep 5(1):70-76.

Hoffmann RF, Zarrintan S, Brandenburg SM, Kol A, de Bruin HG, Jafari S, Dijk F, Kalicharan D, Kelders M, Gosker HR, Ten Hacken NH, van der Want JJ, van Oosterhout

878 AJ, Heijink IH (2013) Prolonged cigarette smoke exposure alters mitochondrial structure
879 and function in airway epithelial cells. Respir Res 14(97):1-12.
880 Holmström KM, Kostov RV, Dinkova-Kostova AT (2016) The multifaceted role of Nrf2 in
881 mitochondrial function, Curr Opinion Toxicol 1:80-91.
882 Jiang Y, Wang X, Hu D (2017) Mitochondrial alterations during oxidative stress in chronic
883 obstructive pulmonary disease. Int J COPD 12:1153-1162.
884 Jin X, Xue B, Zhou Q, Su R, Li Z (2018) Mitochondrial damage mediated by ROS incurs
885 bronchial epithelial cell apoptosis upon ambient PM2.5 exposure. The Journal of
886 Toxicological Sciences 43(2):101-111.
887 Karoui A, Crochemore C, Mulder P, Preterre D, Cazier F, Dewaele D, Corbière C, Mekki M,
888 Vendeville C, Richard V, Vaugeois JM, Fardel O, Sichel F, Lecureur V, Monteil C (2019)
889 An integrated functional and transcriptomic analysis reveals that repeated exposure to
890 diesel exhaust induces sustained mitochondrial and cardiac dysfunctions. Environmental
891 Pollution, 246:518-526.
892 Kim H, Kim H, Park Y, Lee JT (2017) Assessment of temporal variation for the risk of
893 particulate matters on asthma hospitalization. Environ Res 156:542-550.
894 Lavrich KS, Corteselli EM, Wages PA, Bromberg PA, Simmons SO, Gibbs-Flournoy EA,
895 Samet JM (2018) Investigating mitochondrial dysfunction in human lung cells exposed to
896 redox-active PM components. Toxicology and Applied Pharmacology 342:99-107.
897 Leclercq B, Happillon M, Antherieu S, Hardy EM, Alleman LY, Grova N, Perdrix E,
898 Appenzeller BM, Lo Guidice J-M, Coddeville P, Garçon G (2016) Differential responses
899 of healthy and chronic obstructive pulmonary diseased human bronchial epithelial cells
900 repeatedly exposed to air pollution-derived PM_4. Env Poll 218:1074-1088.
901 Leclercq B, Platel A, Antherieu S, Alleman LY, Hardy E,M, Perdrix E, Grova N, Riffault V,
902 Appenzeller BM, Happillon M, Neslany F, Coddeville P, Lo Guidice J-M, Garçon G

(2017a) Genetic and epigenetic alterations in normal and sensitive COPD-diseased human bronchial epithelial cells repeatedly exposed to air pollution-derived $PM_{2,5}$. Env Poll 230:163-177.

Leclercq B, Alleman LY, Perdrix E, Riffault V, Happillon M, Strecker A, Lo Guidice J-M, Garçon G, Coddeville P (2017b) Particulate metal bioaccessibility in physiological fluids and cell culture media: Toxicological perspectives? Env Res 156:148-157.

Leclercq B, Kluza J, Antherieu S, Sotty J, Alleman LY, Perdrix E, Loyens A, Coddeville P, Lo Guidice JM, Marchetti P, Garçon G (2018) Air pollution-derived $PM_{2.5}$ impairs mitochondrial function in healthy and chronic obstructive pulmonary diseased human bronchial epithelial cells. Environ Pollut. 243(PtB):1434-1449.

Lerner CA, Sundar IK, Rahman I (2016) Mitochondrial redox system, dynamics, and dysfunction in lung inflammaging and COPD. The International Journal of Biochemistry & Cell Biology 81:294-306.

Li N, Sioutas C, Cho A, Schmitz D, Misra C, Sempf J, Wang M, Oberley T, Froines J, Nel A (2003) Ultrafine particulate pollutants induce oxidative stress and mitochondrial damage. Environ Health Perspect 111(4):455-460.

Li R, Kou X, Geng H, Xie J, Yang Z, Zhang Y, Cai Z, Dong C (2015) Effect of Ambient PM 2.5 on Lung Mitochondrial Damage and Fusion/Fission Gene Expression in Rats. Chem. Res. Toxicol 28(3):408-418.

Liu J, Liang S, Du Z, Zhang J, Sun B, Zhao T, Yang X, Shi Y, Duan J, Sun Z (2019) PM2.5 aggravates the lipid accumulation, mitochondrial damage and apoptosis in macrophage foam cells. Environmental Pollution 249:482-490.

Longhin E, Pezzolato E, Mantecca P, Holme JA, Franzetti A, Camatini M, Gualtieri M (2013) Season linked responses to fine and quasi-ultrafine Milan PM in cultured cells. Toxicol *in vitro* 27:551-559.

928 Longhin E, Capasso L, Battaglia C, Proverbio M,C, Consentino C, Cifola I, Mangano E,
929 Camatini M, Gualtieri M (2016) Integrative transcriptomic and protein analysis of human
930 bronchial BEAS-2B exposed to seasonal urban particulate matter. Environ Poll 209:87-98
931 Loomis D, Grosse Y, Lauby-Secretan B, El Ghissassi F, Bouvard V, Benbrahim-Tallaa L,
932 Guha N, Baan R, Mattock H, Straif K on behalf of the International Agency for Research
933 on Cancer. Monograph Working Group IARC, Lyon, France (2013) Lancet Oncol
934 14:1262-1263
935 Malinska D, Szymański J, Patalas-Krawczyk P, Michalska B, Wojtala A, Prill M, Partyka M,
936 Drabik K, Walczak J, Sewer A, Johne S, Luettich K, Peitsch MC, Hoeng J, Duszyński J,
937 Szczepanowska J, van der Toorn M, Wieckowski MR (2018) Assessment of mitochondrial
938 function following short- and long-term exposure of human bronchial epithelial cells to
939 total particulate matter from a candidate modified-risk tobacco product and reference
940 cigarettes. Food and Chemical Toxicology 115:1-12.
941 Mbengue S, Alleman LY, Flament P (2014) Size-distributed metallic elements in submicronic
942 and ultrafine atmospheric particles from urban and industrial areas in northern France.
943 Atmos Res 135-136:35-47.
944 Meyer A, Laverny G, Bernardi L, Charles AL, Alsaleh G, Pottecher J, Sibilia J, Geny B
945 (2018) Mitochondria: An Organelle of Bacterial Origin Controlling Inflammation. Front
946 Immunol 9:536.
947 Mirabelli MC, Vaidyanathan A, Flanders WD, Qin X, Garbe P (2016) Outdoor $PM_{2.5}$,
948 Ambient Air Temperature, and Asthma Symptoms in the Past 14 Days among Adults with
949 Active Asthma. Environ. Health Perspect 124(12):1882-1890.
950 Pardo M, Katra I, Schaeur JJ, Rudich Y (2017) Mitochondria-mediated oxidative stress
951 induced by desert dust in rat alveolar macrophages: Desert Dust Damages Mitochondria
952 Function. GeoHealth 1(1) 4-16.

953 Pardo M, Xu F, Shemesh M, Qiu X, Barak Y, Zhu T, Rudich Y (2019) Nrf2 protects against
954 diverse PM2.5 components-induced mitochondrial oxidative damage in lung cells. Sci
955 Total Environ. 669:303-313.
956 Petrosillo G, Ruggiero FM, Pistolese M, Paradies G (2001) Reactive oxygen species
957 generated from the mitochondrial electron transport chain induce cytochrome c
958 dissociation from beef-heart submitochondrial particles via cardiolipin peroxidation.
959 Possible role in the apoptosis. FEBS Letters 509(3):435-438.
960 Piantadosi CA, Carraway MS, Babiker A, Suliman HB. 2008. Heme oxygenase-1 regulates
961 cardiac mitochondrial biogenesis via Nrf2-mediated transcriptional control of nuclear
962 respiratory factor-1. Circ Res. 103(11), 1232-1240.
963 Platel A, Privat K, alahari S, Delobel A, Dourdin G, Gateau E, Simar S, Saleh Y, Sotty J,
964 Antherieu S, Canivet L, Alleman L-Y, Perdrix E, Garçon G, Denayer F-O, Lo Guidice J-
965 M, Nesslany F (2020) Study of in vitro and in vivo genotoxic effects of air pollution fine
966 ($PM_{2.5-0.18}$) and quasi-ultrafine ($PM_{0.18}$) particles on lung models. Sci Total Environ.
967 711:134666.
968 Raaschou-Nielsen O, Beelen R, Wang M et al. (2016) Particulate matter air pollution
969 components and risk for lung cancer. Environ Int 87:66-73.
970 Reddy PH (2011) Mitochondrial Dysfunction and Oxidative Stress in Asthma: Implications
971 for Mitochondria-Targeted Antioxidant Therapeutics Pharmaceuticals (Basel)
972 4(3):429-456.
973 Saint-Georges F, Abbas I, Verdin A, Gosset P, Mulliez P, Shirali P, Garçon G (2008) Gene
974 expression induction of volatile organic compound and/or polycyclic aromatic
975 hydrocarbon-metabolizing enzymes in isolated human alveolar macrophages in response to
976 airborne particulate matter $PM_{2,5}$. Toxicology 244:220-230.

977 Saint-Georges F, Garçon G, Escande F, Abbas I, Verdin A, Gosset P, Mulliez P, Shirali P
978 (2009) Role of air pollution particulate matter ($PM_{2,5}$) in the occurrence of loss of
979 heterozygosity in multiple critical regions of 3p chromosome in human epithelial lung cells
980 L132. Toxicol Lett 187:172-179
981 Saleh Y, Antherieu S, Dusautoir R, Y Alleman L, Sotty J, De Sousa C, Platel A, Perdrix E,
982 Riffault V, Fronval I, Nesslany F, Canivet L, Garçon G, Lo-Guidice JM (2019) Exposure
983 to atmospheric ultrafine particles induces severe lung inflammatory response and tissue
984 remodeling in mice. Int J Environ Res Public Health. 4;16 (7).
985 Scarpulla RC (2008) Nuclear Control of Respiratory Chain Expression by Nuclear
986 Respiratory Factors and PGC-1-Related Coactivator. Ann N Y Acad Sci 1147:321-334.
987 Schroedl C, McClintock DS, Budinger GRS, Chandel NS (2002) Hypoxic but not anoxic
988 stabilization of HIF-1α requires mitochondrial reactive oxygen species. American Journal
989 of Physiology-Lung Cellular and Molecular Physiology 283(5):922-931.
990 Sotty J, Garçon G, Denayer FO, Alleman LY, Saleh Y, Perdrix E, Riffault V, Dubot P, Lo-
991 Guidice JM, Canivet L (2019) Toxicological effects of ambient fine ($PM_{2.5-0.18}$) and
992 ultrafine ($PM_{0.18}$) particles in healthy and diseased 3D organo-typic mucocilary-phenotype
993 models. Environ Res. 176:108538.
994 Stone V, Miller MR, Clift MJD, Elder A, Mills NL, Møller P, Schins RPF, Vogel U, Kreyling
995 WG, Alstrup Jensen K, Kuhlbusch TAJ, Schwarze PE, Hoet P, Pietroiusti A, De Vizcaya-
996 Ruiz A, Baeza-Squiban A, Teixeira JP, Tran CL, Cassee FR (2017) Nanomaterials versus
997 ambient ultrafine particles: an opportunity to exchange toxicology knowledge. Environ
998 Health Perspect. 125(10):106002.
999 Stotland A, Gottlieb RA. (2015) Mitochondrial quality control: Easy come, easy go. Biochim
1000 Biophys Acta. 1853(10 Pt B):2802-2811.

1001 Suzuki M, Otsuki A, Keleku-Lukwete N, Yamamoto M (2016) Overview of redox regulation
1002 by Keap1–Nrf2 system in toxicology and cancer. Curr Opinion Toxicol 1:29-36.
1003 Tilokani L, Nagashima S, Paupe V, Prudent J (2018) Mitochondrial dynamics: overview of
1004 molecular mechanisms. Essays Biochem. 62(3):341-360.
1005 Upadhyay D, Panduri V, Ghio A, Kamp DW (2003) Particulate Matter Induces Alveolar
1006 Epithelial Cell DNA Damage and Apoptosis. Am J Respir Cell Mol Biol 29(2):180-187.
1007 Vales G, Rubio L, Marcos R (2015) Long-term exposures to low doses of titanium dioxide
1008 nanoparticles induce cell transformation but not genotoxic damage in BEAS-2B cells.
1009 Nanotoxicology 9:568-578.
1010 Vucic EA, Chari R, Thu KL, Wilson IM, Cotton AM, Kennett JY, Zhang M, Lonergan KM,
1011 Steiling K, Brown CJ, McWilliams A, Ohtani K, Lenburg ME, Sin DD, Spira A,
1012 MacAulay CE, Lam S, Lam WL (2014) DNA methylation is globally disrupted and
1013 associated with expression changes in chronic obstructive pulmonary disease small
1014 airways. Am J Respir Cell Mol Biol 50(5):912-922.
1015 Wang Y, Zhang M, Li Z, Yue J, Xu M, Zhang Y, LamYung KK, Li R (2019) Fine particulate
1016 matter induces mitochondrial dysfunction and oxidative stress in human SH-SY5Y cells .
1017 Chemosphere 218:577-588.
1018 Wardyn JD, Ponsford AH, Sanderson CM (2015) Dissecting molecular cross-talk between
1019 Nrf2 and NF-κB response pathways. Biochem, Soc, Trans 43:621-626.
1020 Wiegman CH, Michaeloudes C, Haji G, Narang P, Clarke CJ, Russell KE, Bao W, Pavlidis S,
1021 Barnes PJ, Kanerva J, Bittner A, Rao N, Murphy MP, Kirkham PA, Chung KF, Adcock IM
1022 (2015) Oxidative stress–induced mitochondrial dysfunction drives inflammation and
1023 airway smooth muscle remodeling in patients with chronic obstructive pulmonary disease.
1024 Journal of Allergy and Clinical Immunology 136(3):769-780.

1025 Willems PH, Rossignol R, Dieteren CE, Murphy MP, Koopman WJ. (2015). Redox
1026 homeostasis and mitochondrial dynamics. Cell Metab. 22(2):207-218.

1027 Winckelmans E, Nawrot TS, Tsamou M, Den Hond E, Baeyens W, Kleinjans J, Lefebvre W,
1028 Van Larebeke N, Peusens M, Plusquin M, Reynders H, Schoeters G, Vanpoucke C, de Kok
1029 TM, Vrijens K (2017) Transcriptome-wide analyses indicate mitochondrial responses to
1030 particulate air pollution exposure. Environ Health 16(1):87.

1031 Wu Z, Puigserver P, Andersson U, Zhang C, Adelmant G, Mootha V, Troy A, Cinti S, Lowell
1032 B, Scarpulla RC, Spiegelman BM (1999) Mechanisms Controlling Mitochondrial
1033 Biogenesis and Respiration through the Thermogenic Coactivator PGC-1. Cell 98(1)-
1034 115-124.

1035 Xu Y, Lindh CH, Jönsson BAG, Broberg K, Albin M, (2018) Occupational exposure to
1036 asphalt mixture during road paving is related to increased mitochondria DNA copy
1037 number: a cross-sectional study. Environmental Health 17(1):29.

1038 Yang X, Feng L, Zhang Y, Hu H, Shi Y, Liang S, Zhao T, Fu Y, Duan J, Sun Z (2018)
1039 Cytotoxicity induced by fine particulate matter ($PM_{2.5}$) via mitochondria-mediated
1040 apoptosis pathway in human cardiomyocytes. Ecotoxicology and Environmental Safety
1041 161-198-207.

1042 Youle RJ, van der Bliek AM (2012) Mitochondrial Fission, Fusion, and Stress. Science
1043 337(6098):1062-1065.

1044 Zheng L, Liu S, Zhuang G, Xu J, Liu Q, Zhang X, Deng C, Guo Z, Zhao W, Liu T, Wang Y,
1045 Zhang Y, Lin J, Wang Q, Sui G (2017) Signal transductions of BEAS-2B cells in response
1046 to carcinogenic $PM_{2,5}$ exposure based on a microfluidic system. Anal Chem 89:5413-5421

1047 Zhou R, Yazdi AS, Menu P, Tschopp J (2011) A role for mitochondria in NLRP3
1048 inflammasome activation. Nature 469(7329):221-225.

1049 Zhou W, Tian D, He J, Zhang L, Tang X, Zhang L, Wang Y, Li L, Zhao J, Yuan X, Peng S
1050 (2017) Exposure scenario: Another important factor determining the toxic effects of $PM_{2,5}$
1051 and possible mechanisms involved. Env Poll. 226:412-425.
1052 Zorov DB, Vorobjev IA, Popkov VA, Babenko VA, Zorova LD, Pevzner IB, Silachev DN,
1053 Zorov SD, Andrianova NV, Plotnikov EY. (2019) Lessons from the discovery of
1054 mitochondrial fragmentation (fission): A review and update. Cells 8(2): E175.
1055

FIGURE LEGENDS

Figure 1: Global strategy of the acute or the repeated exposures of human bronchial epithelial BEAS-2B cells to fine or quasi-ultrafine particles (FP or Q-UFP, respectively).

Figure 2: Immunofluorescence labelling of apoptotic cells using TdT-mediated dUTP Nick-End Labeling (TUNEL) (Figure 2-A), capsase-8, -9, and -3/7 activities (Figure 2-B), and immunofluorescence labelling of live cells using SYTOX® Red by flow cytometry (Figure 2-C) in human bronchial epithelial BEAS-2B cells, grown submerged, as negative control, or acutely (1 exposure) or repeatedly (3 exposures) incubated with 5 µg/cm² of ambient fine or quasi-ultrafine particles (FP and Q-UFP, respectively). Positive controls for TUNEL method, caspase activity assays, and cell viability assay were treated with DNase I (10 IU/mL, 30 min, 37°C), H_2O_2 (50 µM, 24 h, 37°C, 5% CO_2), and menadione (100 µM, 4 h, 37°C, 5% CO_2), respectively. Values are depicted as means and standard deviations (n = 3). (T test; **: $p < 0.01$ vs negative control cells).

Figure 3: Mitochondrial membrane potential (ΔΨm), using the fluorescent dye tetramethylrhodamine, methyl ester, perchlorate (TMRM) (Figures 3-A and 3-B), and ATP intracellular contents, using CellTiter-Glo® Luminescent cell viability assay (Figure 3-C, 3-D), in human bronchial epithelial BEAS-2B cells, grown submerged, as negative control, or acutely (1 exposure) or repeatedly (3 exposures) incubated with 5 µg/cm² or ranging concentrations from 0.5 to 50 µg/cm² of ambient fine or quasi-ultrafine particles (FP and Q-UFP, respectively). Carbonyl cyanide-4-(trifluoromethoxy)phenylhydrazone (FCCP; 25 µM, 30 min, , 5% CO_2), a protonophore that uncouples oxidation from phosphorylation by dissipating the chemiosmotic gradient and induces dissipation of ΔΨm, was used as positive

control. Values are depicted as means and standard deviations (n = 3). (T test; *: $p < 0.05$ and **: $p < 0.01$, vs control cells).

Figure 4: Oxygen consumption rates (OCR) in human bronchial epithelial BEAS-2B cells, grown submerged, as negative control, or acutely (1 exposure; Figures 4-A and 4-C) or repeatedly (3 exposures; Figures 4-B and 4-D) incubated with 5 µg/cm² of ambient fine or quasi-ultrafine particles (FP and Q-UFP, respectively). Figures 4-A and 4-B show OCR as studied using the Seahorse XF24 Extracellular Flux Analyser after the sequential addition of oligomycin (Oli, 1 µM), 2-[2-(3-Chlorophenyl) hydrazinylyidene]propanedinitrile (FCCP; 0.25-0.5 µM), rotenone (i.e., Rot, 1 µM), and antimycin A (AA, 1 µM). As shown by Figures 4-C and 4-D, the different states of mitochondrial respiration are depicted as follow: basal respiration (basal), proton leak (respiration after Oli addition), maximal respiratory capacity (i.e., respiration after FCCP addition), and non-mitochondrial respiration (i.e., after Rot/AA addition). Figures 4-C and 4-B show non-mitochondrial respiration, basal respiration, proton leaked linked respiration, ATP leaked linked respiration, and reserve capacity, based on data gathered from the Seahorse XF24 Extracellular Flux Analyses. Values are depicted as means and standard deviations (n = 3). (T test; *: $p < 0.05$ and **: $p < 0.01$, vs control cells).

Figure 5: All the mitochondrial electron transport chain (ETC) complex subunits (i.e., CI-NDUFB8, CII-SDBH, CIII-UQCRC2, CIV-MT-CO1, and CV-ATPSA; Figures 5-A, 5-B, and 5-C), and mitochondrial porins (i.e., translocase of outer mitochondrial membrane 20: TOMM20, and voltage dependent anion channel: VDAC; Figure 5-D) in human bronchial epithelial BEAS-2B cells, grown submerged, as negative control, or acutely (1 exposure) or repeatedly (3 exposures) incubated with 5 µg/cm² of ambient fine or quasi-ultrafine particles (FP and Q-UFP, respectively). The protein relative intensity of the ETC complex subunits are

expressed vs β-actin (Figure 5-B) and vs TOMM20 (Figure 5-C), as mitochondrial mass marker. Values are depicted as means and standard deviations (n = 3). (T test; *: $p < 0.05$ and **: $p < 0.01$, vs control cells).

Figure 6: ROS generation, using the fluorescent dye MitoSOX™ Red (Figures 6-A, 6-B, and 6-C) and the fluorescent dye MitoTracker™ Green (Figure 6-A) in human bronchial epithelial BEAS-2B cells, grown submerged, as negative control, or acutely (1 exposure, Figures 6-B and 6-D) or repeatedly (3 exposures, 6-A; 6-B, and 6-C) incubated with 5 µg/cm² of ambient fine or quasi-ultrafine particles (FP and Q-UFP, respectively). Calculated corrected total cell fluorescence for MitoSOX™ for BEAS-2B cells repeatedly exposed to FP and Q-UFP were 21.36 ± 2.98 and 26.97 ± 3.44, respectively (vs control BEAS-2B cells: 16.77 ± 2.73; $p < 0.01$). Menadione (Mena; 50 µM, 4 h, 37°C, 5% CO_2), a mitochondrial redox cycling promoter, has been used as positive control for ROS generation. Values are depicted as means and standard deviations (n = 3). (T test; *: $p < 0.05$ and **: $p < 0.01$, vs control cells).

Figure 7: Binding activity of nuclear factor erythroid 2 p45-related factor 2 (NRF2) to antioxidant response elements (ARE) (Figure 7-A) and NRF2 target proteins (i.e., NADPH quinone oxido-reductase-1: NQO-1, heme oxygenase: HO-1, and glutamate-cysteine ligase modifier subunit: GLCM; Figure 7-B, 7-C, 7-D, and 7-E) in human bronchial epithelial BEAS-2B cells, grown submerged, as negative control, or acutely (1 exposure) or repeatedly (3 exposures) incubated with 5 µg/cm² of ambient fine or quasi-ultrafine particles (FP and Q-UFP, respectively). Values are depicted as means and standard deviations (n = 3). (T test; *: $p < 0.05$ and **: $p < 0.01$, vs control cells).

Figure 8: Optic atrophy-1 (OPA-1) and mitofusins (mfn1, mfn2), as effector proteins of mitochondrial fusion (Figure 8-A, 8-B), and mitochondrial fission 1 protein (fis1) and dynamin-related protein 1 (drp1 and both its phosphorylated forms: P-drp1 (s616), P-drp-1 (s637)), as effector protein of mitochondrial fission (Figure 8-C, 8-D), in human bronchial epithelial BEAS-2B cells, grown submerged, as negative control, or acutely (1 exposure) or repeatedly (3 exposures) incubated with 5 µg/cm² of ambient fine or quasi-ultrafine particles (FP and Q-UFP, respectively). The accumulation of fis1 on outer mitochondrial membrane allows the recruitment of cytoplasmic protein drp1 to trigger fission process, and the phosphorylation of Drp1 on serine 616 (s616) is known to stimulate mitochondrial fission while its phosphorylation on serine 637 (s637) inhibits it. Mitochondrial network morphology, using the fluorescent dye cell-permeant MitoTracker® red CMXROS probe, which contains a mildly thiol-reactive chloromethyl moiety for labeling mitochondria by passive diffusion across the plasma membrane and accumulation in active mitochondria, in human bronchial epithelial BEAS-2B cells, grown submerged, as negative control or repeatedly (3 exposures) incubated with 5 µg/cm² of ambient FP and Q-UFP (Figure 8-E). Values are depicted as means and standard deviations (n = 3). (T test; *: $p < 0.05$ and **: $p < 0.01$, vs control cells).

Figure 9: Observations of human bronchial epithelial BEAS-2B cells, grown submerged as negative control or repeatedly exposed to 5 µg/cm² of quasi-ultrafine particles (Q-UFP), using transmission electronic microscopy. The presence of some Q-UFP, isolated or even agglomerated, appeared somewhat difficult to observe. In BEAS-2B cell controls, mitochondria were heterogeneous in shape, rounded or elongated, with numerous cristae. Inner and outer mitochondrial membranes appeared intact and the matrix integrity was fully preserved. Like negative control cells, there was no marked mitochondrial abnormality in Q-

UFP-repeatedly exposed BEAS-2B cells, also characterized by the absence of swollen mitochondria with disarrangement and distortion of cristae, and the apparent integrity of the outer membrane.

Figure 10: Dynamics of morphological changes of mitochondria was carefully recorded by the fluorescence labelling with MitoTracker® Red CMXROS probe and the time-lapse videomicroscopy of human bronchial epithelial BEAS-2B cells, grown submerged, as negative control or repeatedly (3 exposures) incubated with 5 µg/cm² of ambient fine or quasi-ultrafine particles (FP and Q-UFP, respectively). Time-lapse video microscopy can be defined as the real time imaging of living cells, which requires both the ability to acquire very rapid events and the signal generated by the observed cellular structure during these events. As shown by the photo series (see also white dotted lines), in repeatedly-exposed BEAS-2B cells to FP and mostly UFP, only a small part of mitochondria was transported over significant distances, while others were in the state of relative rest, as compared to control cells, thereby revealing the reduction of the mitochondrial dynamics, which is the crucial molecular process that maintain the cellular homeostasis selectively removing the damaged mitochondria.

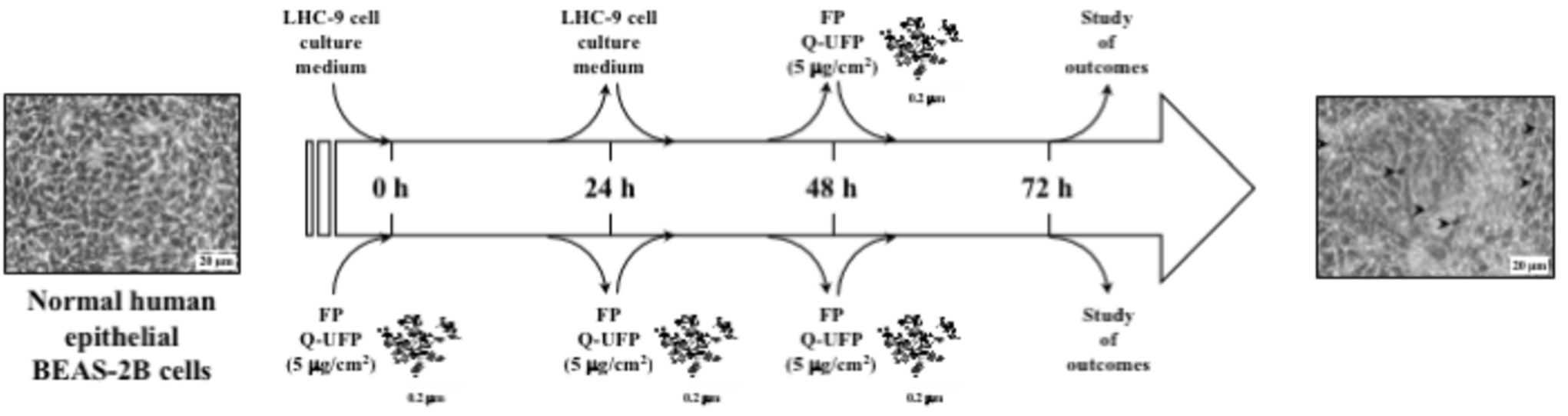
ACUTE EXPOSURE
LHC-9 cell culture medium
LHC-9 cell culture medium
FP Q-UFP (5 µg/cm²)
0.2 µm
Study of outcomes
20 µm
Normal human epithelial BEAS-2B cells
0 h
24 h
48 h
72 h
FP Q-UFP (5 µg/cm²)
0.2 µm
FP Q-UFP (5 µg/cm²)
0.2 µm
FP Q-UFP (5 µg/cm²)
0.2 µm
Study of outcomes
20 µm
REPEATED EXPOSURE

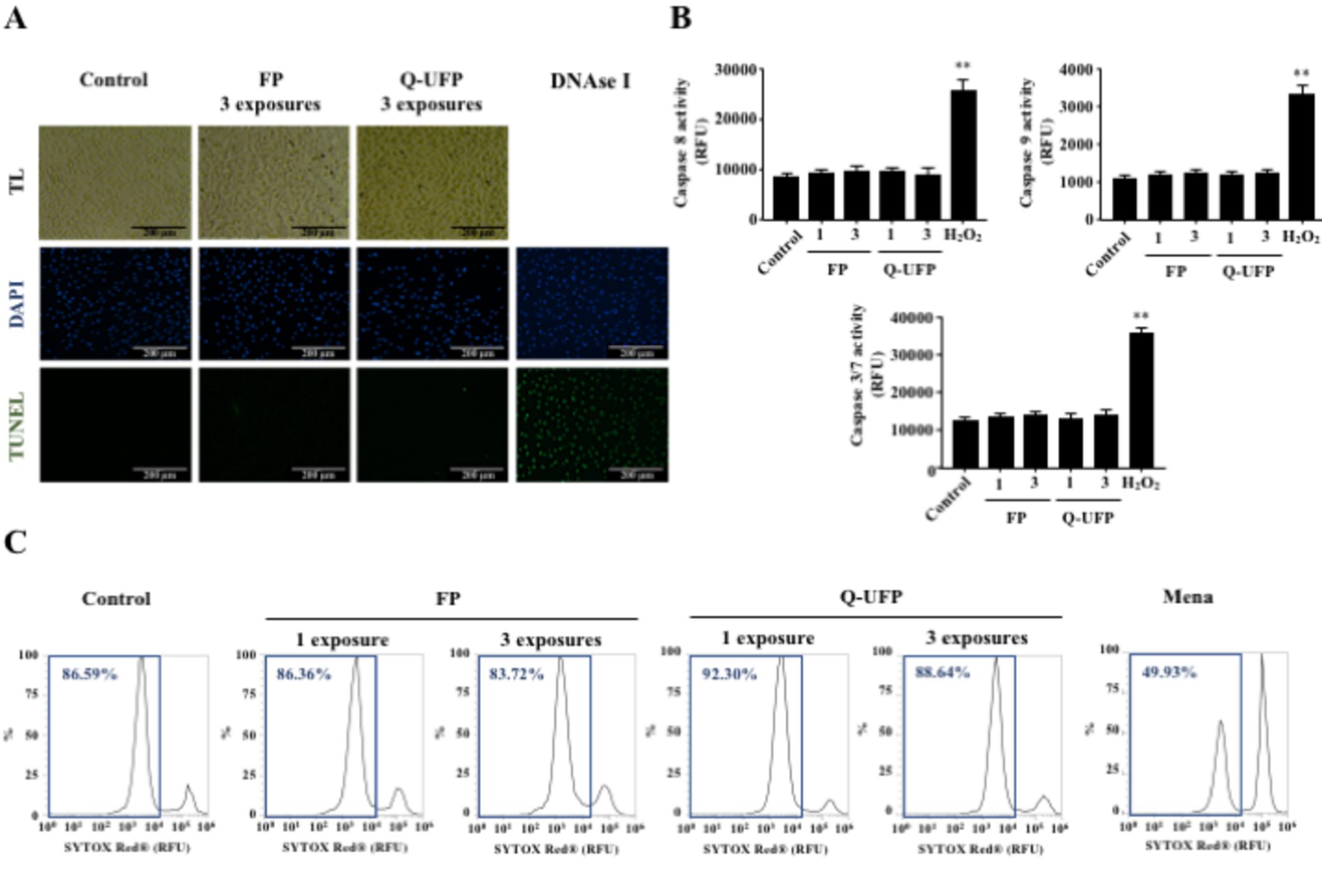
A
Control
FP
3 exposures
Q-UFP
3 exposures
DNAse I
TL
DAPI
TUNEL
200 µm
B
Caspase 8 activity (RFU)
Caspase 9 activity (RFU)
Caspase 3/7 activity (RFU)
Control
1
3
1
3
H2O2
FP
Q-UFP
**
C
Control
FP
Q-UFP
Mena
1 exposure
3 exposures
1 exposure
3 exposures
86.59%
86.36%
83.72%
92.30%
88.64%
49.93%
SYTOX Red® (RFU)

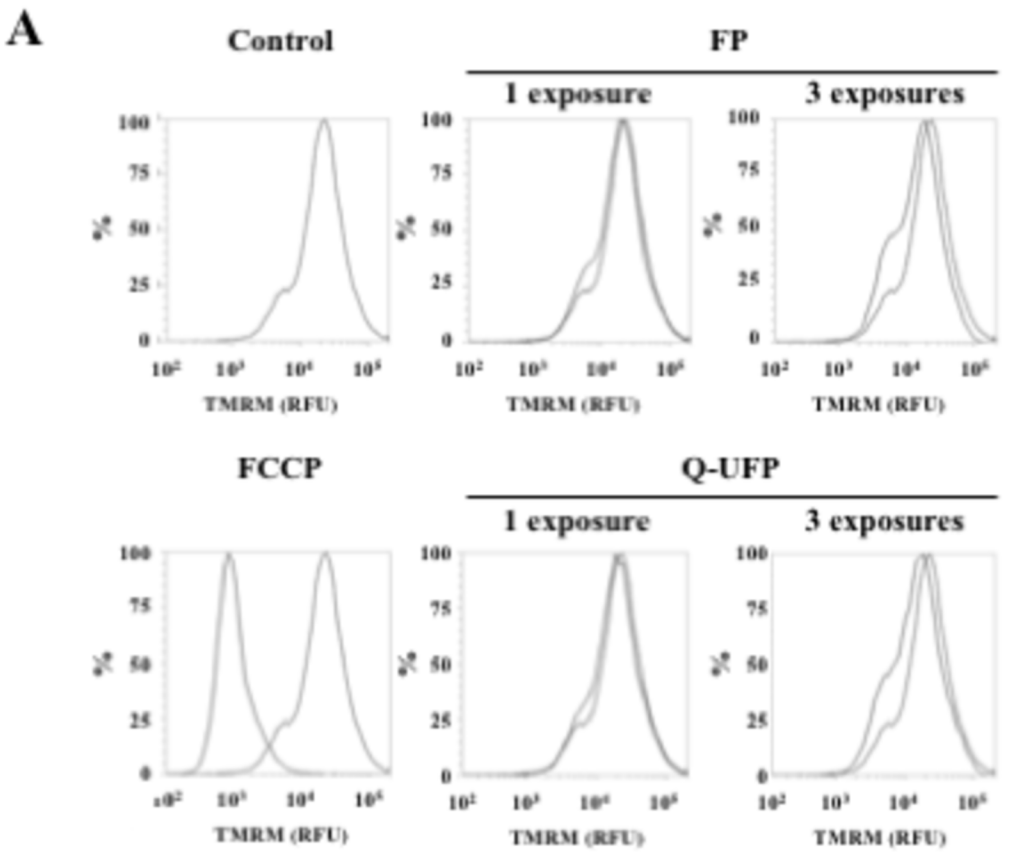
A
Control
FP
1 exposure
3 exposures
FCCP
Q-UFP
1 exposure
3 exposures
%
TMRM (RFU)

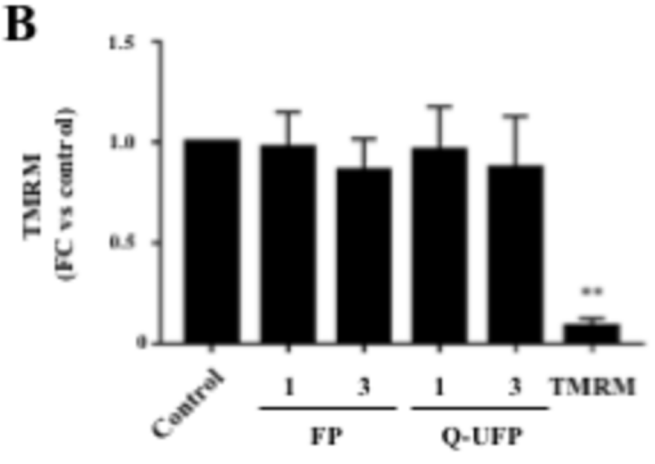
B
TMRM
(FC vs control)
**
Control
1
3
1
3
TMRM
FP
Q-UFP

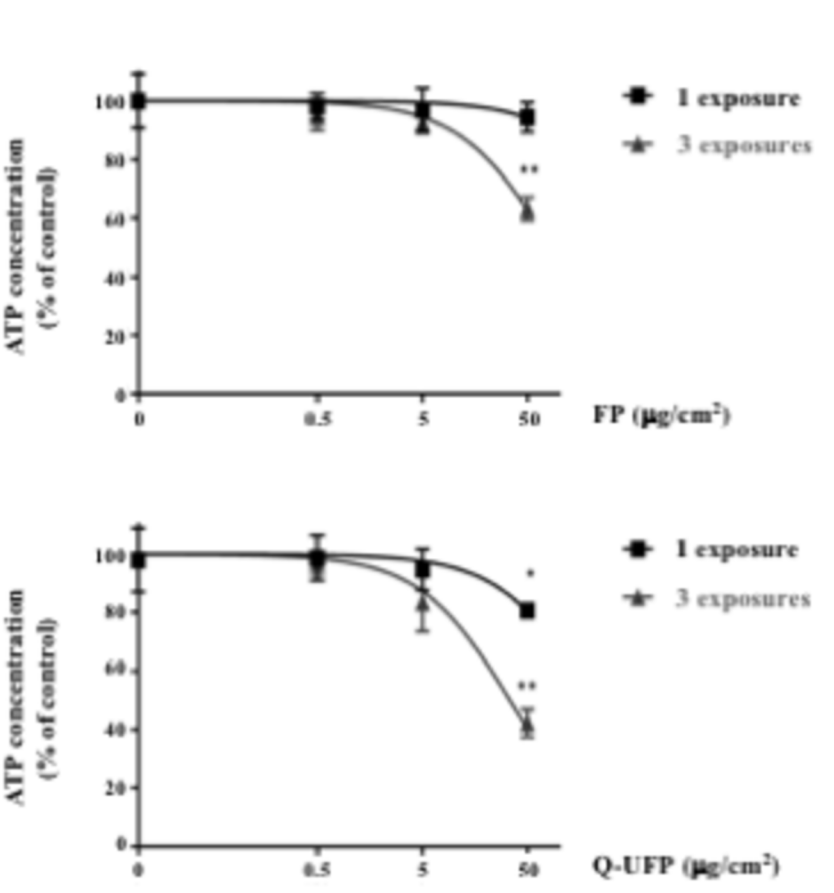
C
ATP concentration
(% of control)
1 exposure
3 exposures
**
FP (µg/cm²)
*
**
Q-UFP (µg/cm²)

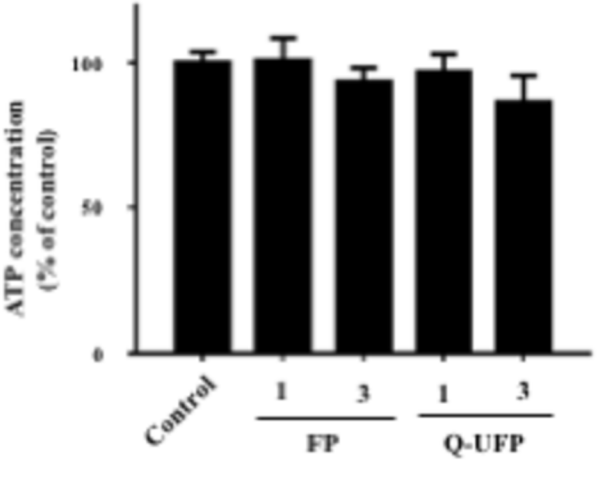
D
ATP concentration
(% of control)
Control
1
3
1
3
FP
Q-UFP

A

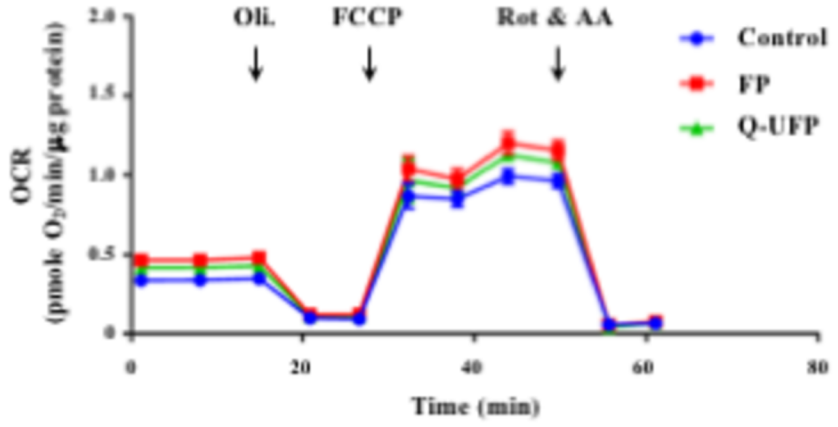
Oli.
FCCP
Rot & AA
Control
FP
Q-UFP
OCR
(pmole O2/min/μg protein)
Time (min)

B

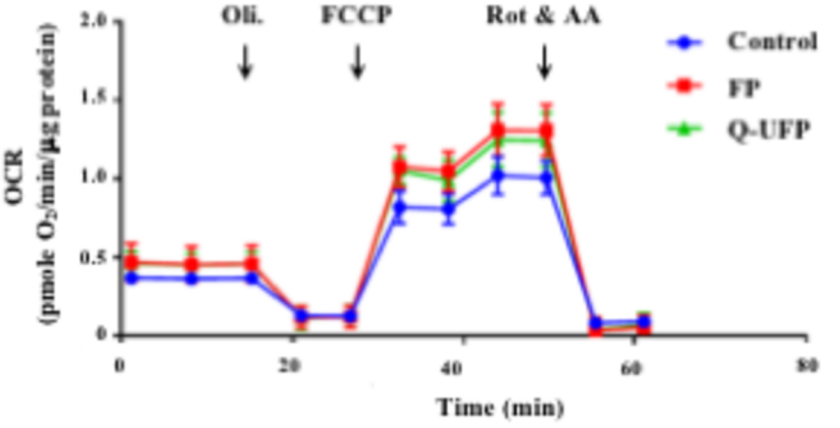
Oli.
FCCP
Rot & AA
Control
FP
Q-UFP
OCR
(pmole O2/min/μg protein)
Time (min)

C

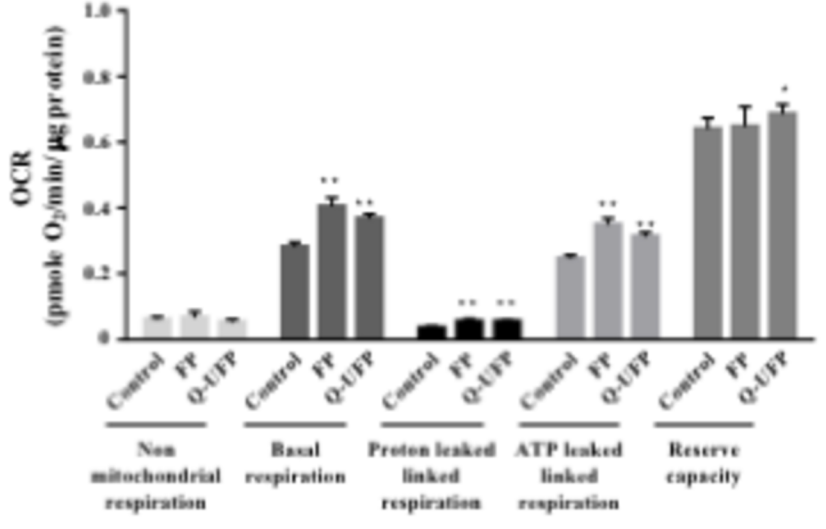
OCR
(pmole O2/min/μg protein)
Control
FP
Q-UFP
Non mitochondrial respiration
Basal respiration
Proton leaked linked respiration
ATP leaked linked respiration
Reserve capacity

D

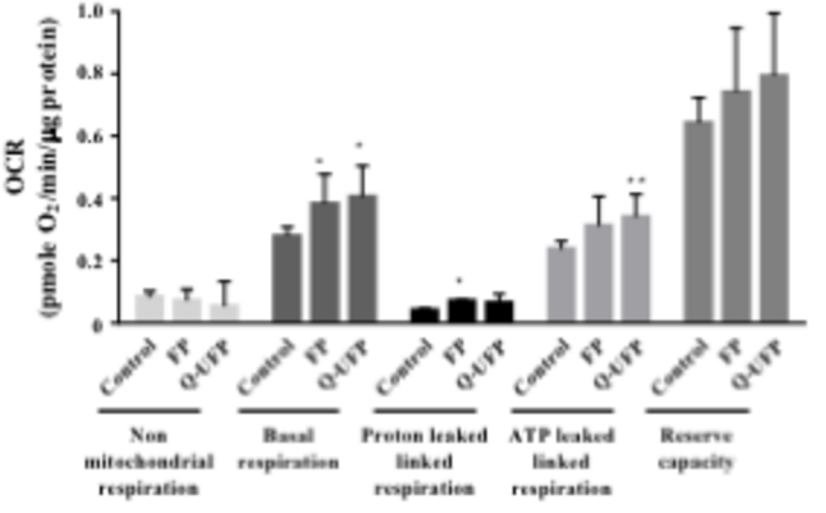
OCR
(pmole O2/min/μg protein)
Control
FP
Q-UFP
Non mitochondrial respiration
Basal respiration
Proton leaked linked respiration
ATP leaked linked respiration
Reserve capacity

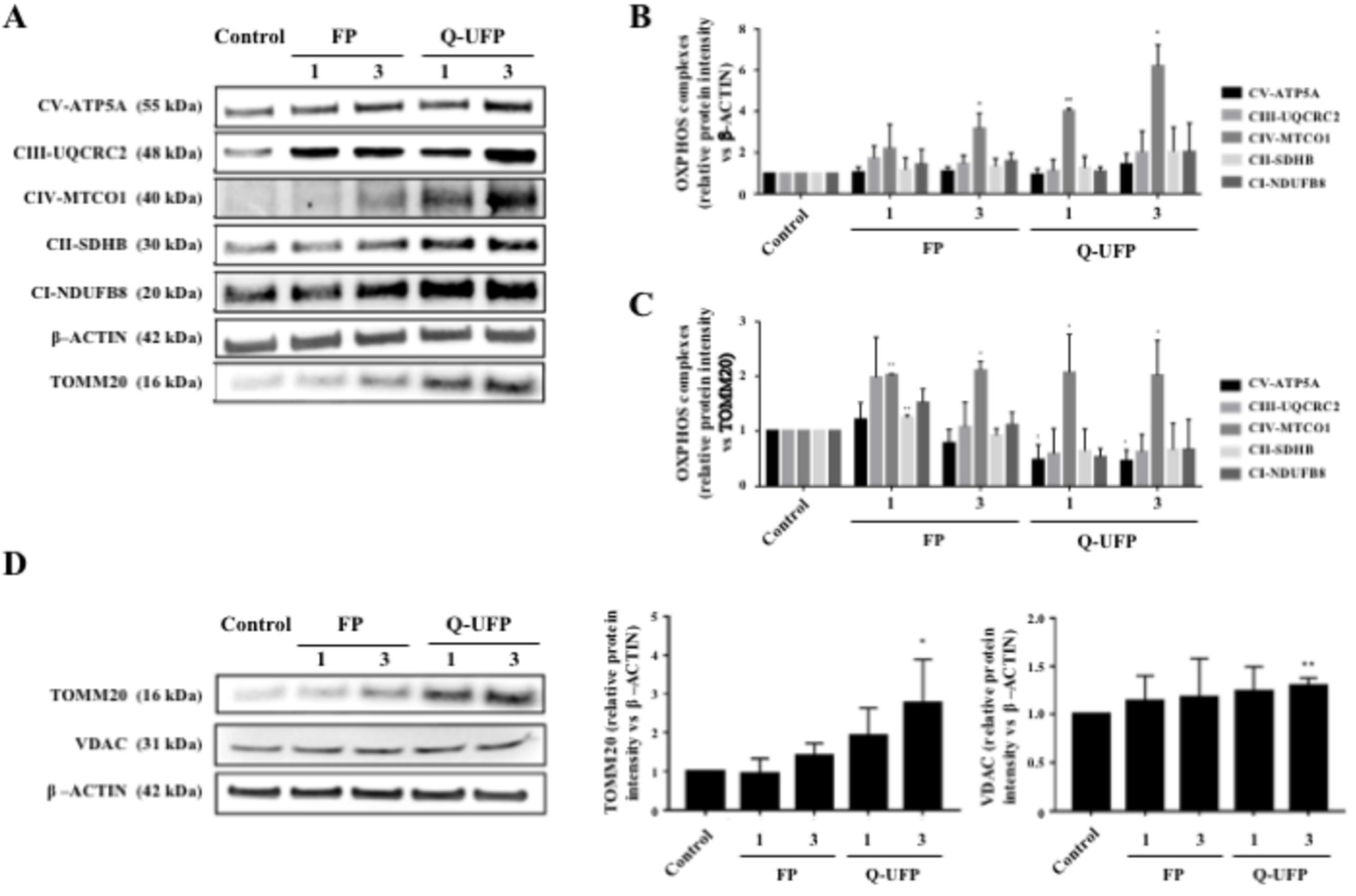
A
Control
FP
Q-UFP
1
3
1
3
CV-ATP5A (55 kDa)
CIII-UQCRC2 (48 kDa)
CIV-MTCO1 (40 kDa)
CII-SDHB (30 kDa)
CI-NDUFB8 (20 kDa)
β–ACTIN (42 kDa)
TOMM20 (16 kDa)
B
OXPHOS complexes (relative protein intensity vs β-ACTIN)
CV-ATP5A
CIII-UQCRC2
CIV-MTCO1
CII-SDHB
CI-NDUFB8
Control
FP
Q-UFP
C
OXPHOS complexes (relative protein intensity vs TOMM20)
D
TOMM20 (16 kDa)
VDAC (31 kDa)
β –ACTIN (42 kDa)
TOMM20 (relative protein intensity vs β –ACTIN)
VDAC (relative protein intensity vs β –ACTIN)

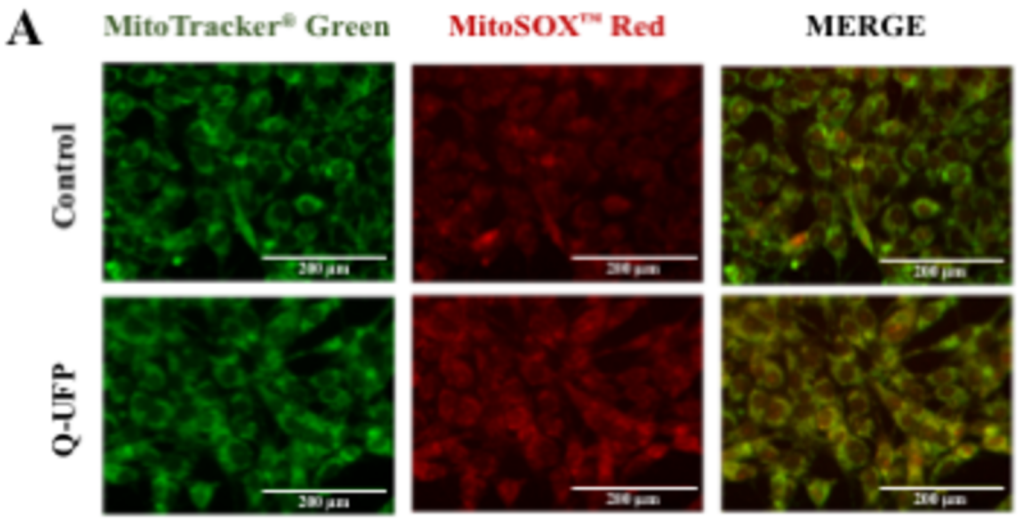
A
MitoTracker® Green
MitoSOX™ Red
MERGE
Control
Q-UFP
200 µm

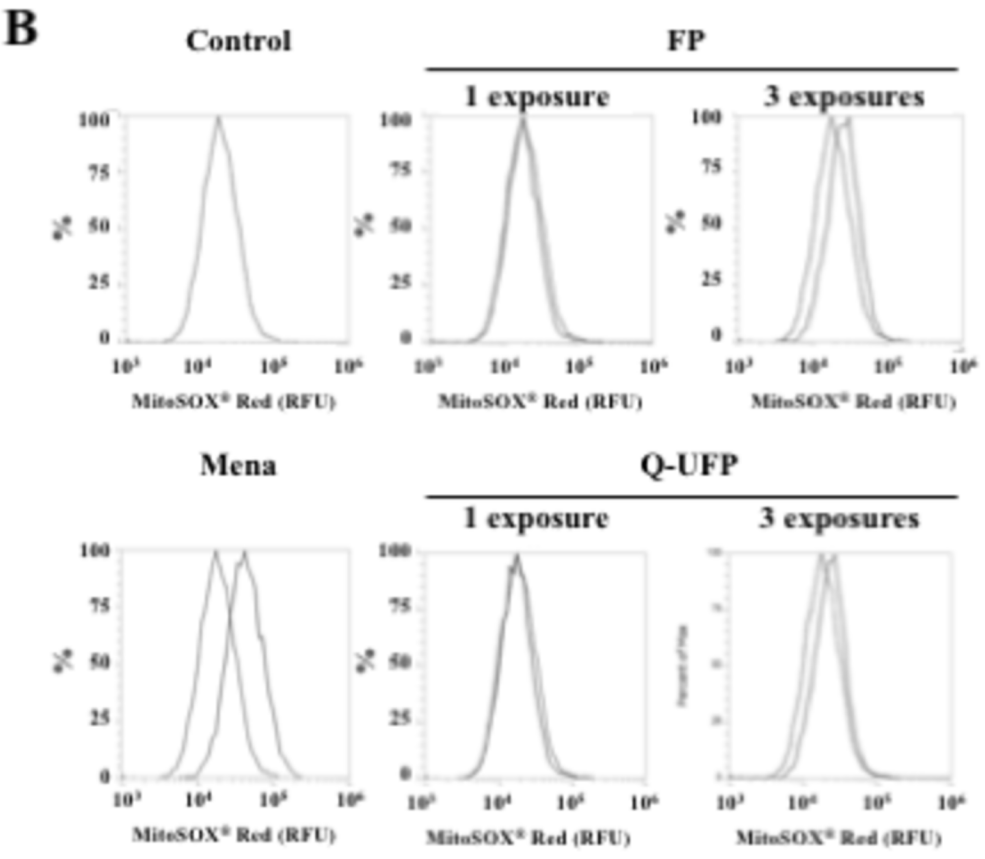
B
Control
FP
1 exposure
3 exposures
Mena
Q-UFP
%
MitoSOX® Red (RFU)

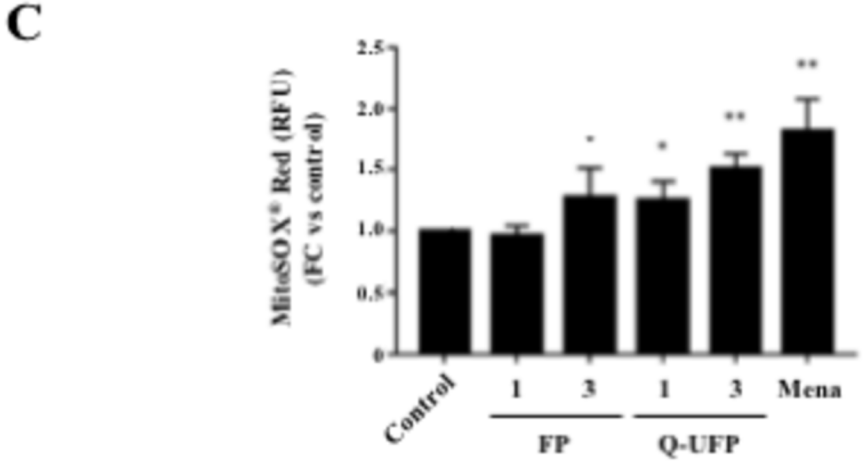
C
MitoSOX® Red (RFU)
(FC vs control)
Control
1
3
1
3
Mena
FP
Q-UFP

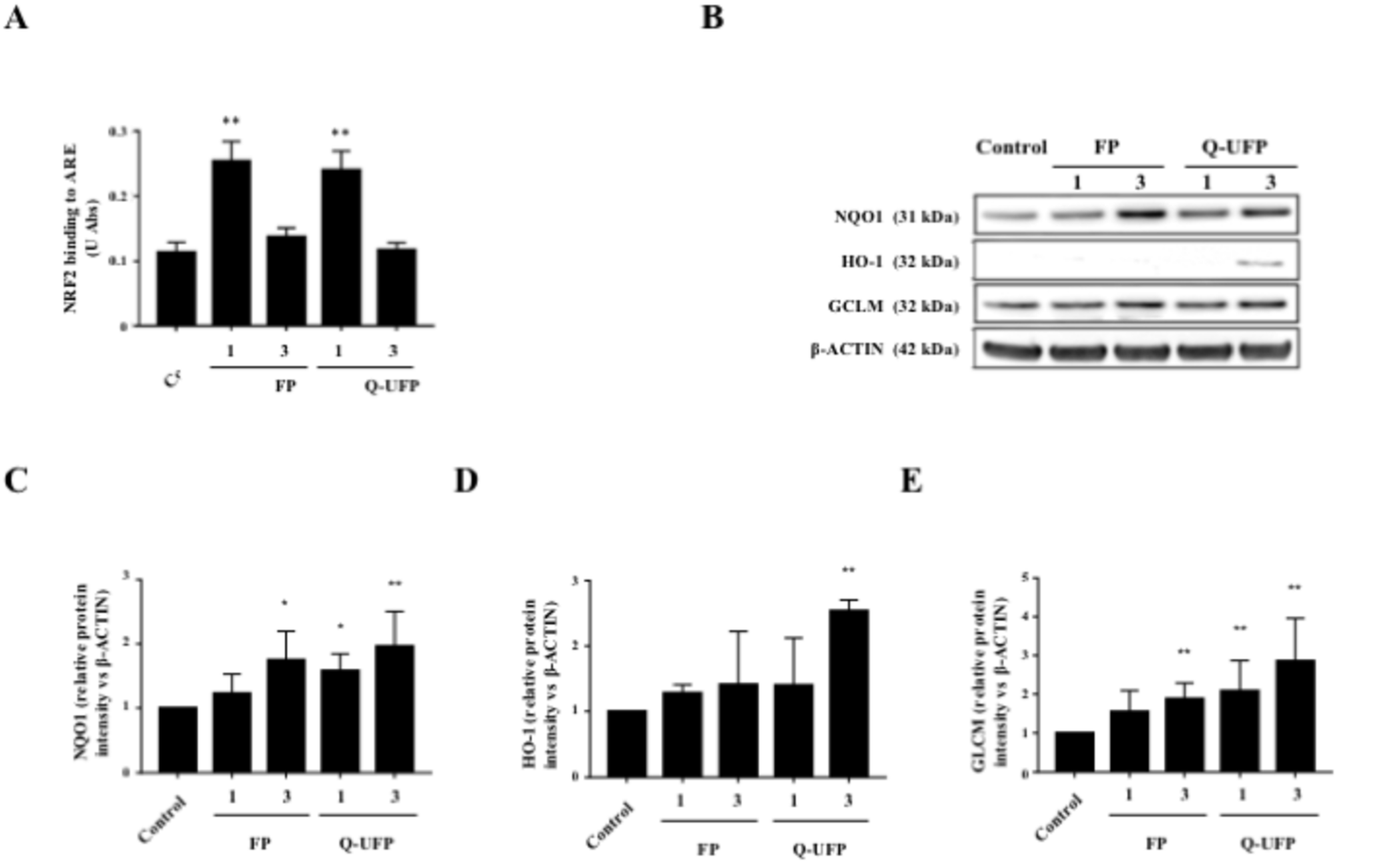
A
NRF2 binding to ARE (U Abs)
0.3
0.2
0.1
0
**
**
1
3
1
3
C
FP
Q-UFP
B
Control
FP
Q-UFP
1
3
1
3
NQO1 (31 kDa)
HO-1 (32 kDa)
GCLM (32 kDa)
β-ACTIN (42 kDa)
C
NQO1 (relative protein intensity vs β-ACTIN)
3
2
1
0
*
*
**
Control
1
3
1
3
FP
Q-UFP
D
HO-1 (relative protein intensity vs β-ACTIN)
3
2
1
0
**
Control
1
3
1
3
FP
Q-UFP
E
GLCM (relative protein intensity vs β-ACTIN)
5
4
3
2
1
0
**
**
**
Control
1
3
1
3
FP
Q-UFP

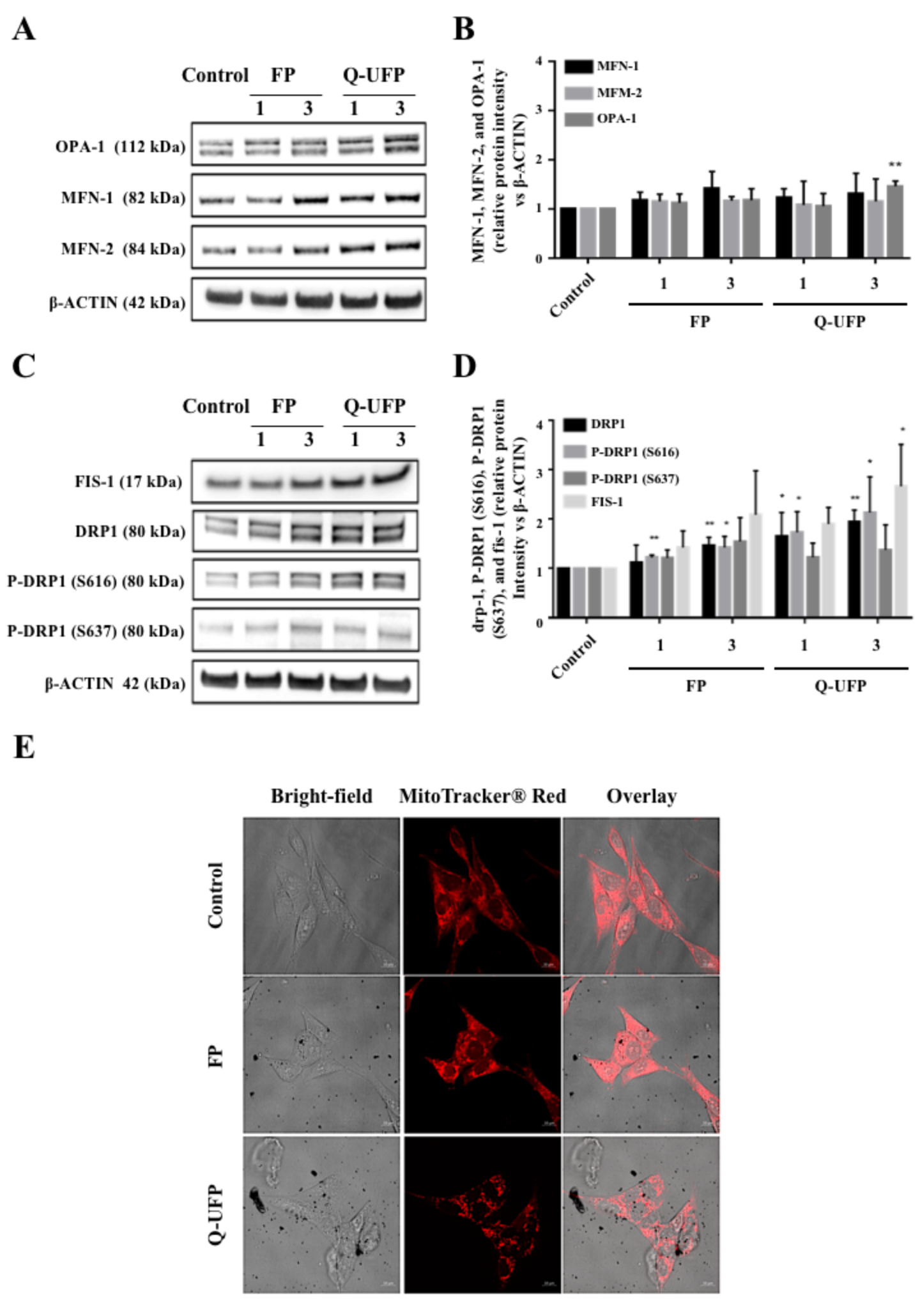
A
Control
FP
Q-UFP
1
3
1
3
OPA-1 (112 kDa)
MFN-1 (82 kDa)
MFN-2 (84 kDa)
β-ACTIN (42 kDa)
B
MFN-1, MFN-2, and OPA-1 (relative protein intensity vs β-ACTIN)
MFN-1
MFM-2
OPA-1
0
1
2
3
4
**
Control
1
3
1
3
FP
Q-UFP
C
Control
FP
Q-UFP
1
3
1
3
FIS-1 (17 kDa)
DRP1 (80 kDa)
P-DRP1 (S616) (80 kDa)
P-DRP1 (S637) (80 kDa)
β-ACTIN 42 (kDa)
D
drp-1, P-DRP1 (S616), P-DRP1 (S637), and fis-1 (relative protein Intensity vs β-ACTIN)
DRP1
P-DRP1 (S616)
P-DRP1 (S637)
FIS-1
0
1
2
3
4
*
**
Control
1
3
1
3
FP
Q-UFP
E
Bright-field
MitoTracker® Red
Overlay
Control
FP
Q-UFP

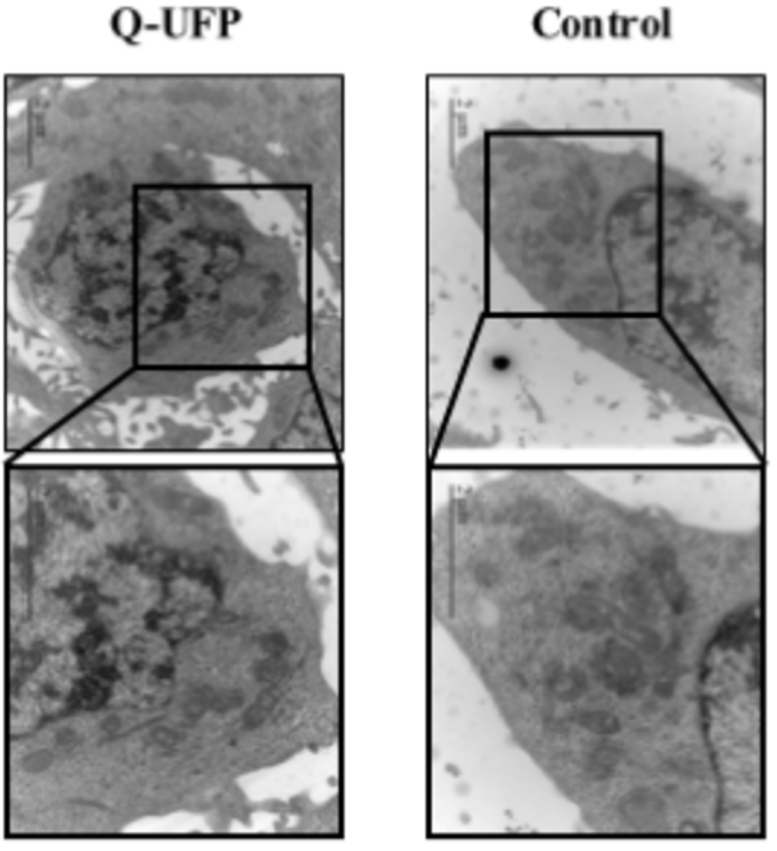
Q-UFP
Control

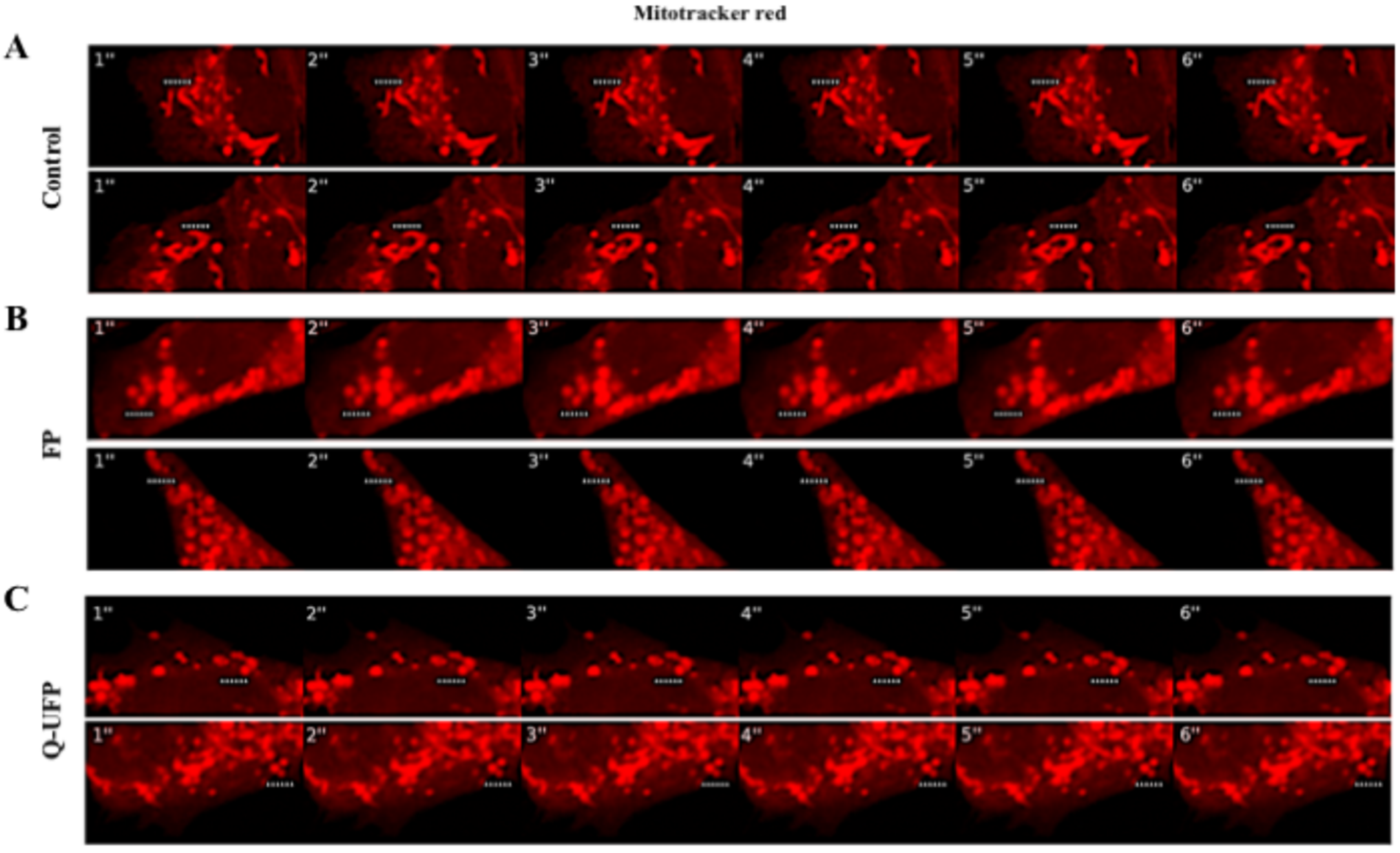
Mitotracker red
A
Control
1''
2''
3''
4''
5''
6''
B
FP
C
Q-UFP

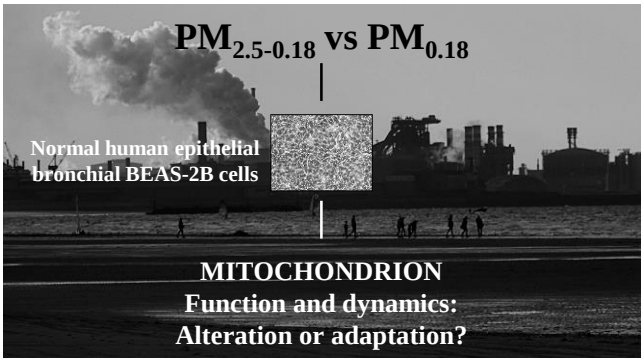
$PM_{2.5-0.18}$ vs $PM_{0.18}$
Normal human epithelial bronchial BEAS-2B cells
MITOCHONDRION
Function and dynamics:
Alteration or adaptation?